

# Probing Surface Structure via Time-of-Escape Analysis of Gas in Knudsen Regime

Renato Feres\* and Gregory Yablonsky†

## Abstract

Continuing the study begun in [FY], we consider transport in the Knudsen regime of inert gases through straight channels and investigate how small-scale surface geometry of a macroscopically flat channel affects the diffusion characteristics of the gas. We show that the diffusivity constant contains information about the surface micro-geometry.

Our investigation is carried out partly by analytical means and also through numerical simulation of what we call *time-of-escape experiment*. This is a type of multi-scattering experiment that measures the mean residence time in channels of varying lengths, allowing for an analysis of the transport process at various stages of development.

We focus attention on the *smoothness constant*  $\xi = D/D_0$ , defined as the ratio of diffusivity for a given micro-geometry,  $D$ , and diffusivity  $D_0$  under “ideal roughness,” i.e., under the assumption that the Knudsen cosine law holds at each collision. The dependence of  $\xi$  on small scale surface morphology is investigated using a variety of parametrized families of micro-geometries. We show that  $\xi$  can tell the presence of certain geometric features, such as curvature or sharp angles at the microscopic level. For example, for a simple 2-D model of atomically smooth surface made of a linear packing of spheres of radius  $R$  probed by gas molecules of radius  $A$  (figure 6), we obtain the approximate relation  $\xi \propto 1 + A/R$ , with a proportionality constant of roughly 1.3. (See section 2 for the range of parameters considered.) This relates to rapid diffusion phenomena recently observed by [Hol]. In the classical collision model of Maxwell-Smoluchowski, with no detailed regard of surface geometry, one always has  $\xi \geq 1$ , but we observe that  $\xi$  can sometimes be less than 1. (Section 2.5.) We obtain exact values for the mean number and duration of collisions as function of the micro-geometry. (Section 3.) This is needed to determine the relative importance of these quantities on diffusivity. We also extend the analysis of the scattering operator of random billiards of [FY] by giving a general criterion for the validity of Knudsen’s cosine law, and describe some of the spectral properties of this operator.

---

\*Washington University, Department of Mathematics, St. Louis, MO 63130

†Washington University, Department of Chemical Engineering, St. Louis, MO 63130

# 1 Theoretical framework

Gas transport in the large Knudsen number limit, or Knudsen regime, is of interest to researchers in many areas of physics, chemistry and technology, from industrial heterogeneous catalytic processes to molecular transport processes in nano-structured materials, to rarified gas processes in atmosphere and space. In this regime, collisions between molecules are rare, so the main contribution to transport characteristics comes from collisions with the wall of the container. This makes it possible in principle to relate the diffusivity constant with morphological details of the wall surface.

The classical expression for Knudsen diffusivity,  $D_0$ , of gas in a capillary tube was derived by Knudsen on the assumption that gas-wall collisions are diffuse and satisfy the so-called *cosine law* [Kn, PP]. Deviations from  $D_0$  are typically expressed as  $D = D_0\xi$ , where  $\xi$  is an empirically determined constant or is derived from additional assumptions about the surface-gas interaction. For example, Smoluchowski generalized Knudsen's result using a model of collision due to Maxwell in which a fraction  $\eta$  of collisions are diffuse, the remaining  $1 - \eta$  being specular. This gives the value of diffusivity

$$D = D_0 \left( \frac{2 - \eta}{\eta} \right).$$

(See, for example, [ACM].) In the present paper, we investigate how the quantity  $\xi$  depends on the surface small scale morphology, or *micro-geometry*.

This is the continuation of a study of gas transport in the Knudsen regime begun in [FY], based on the *random billiard model* of gas-surface interaction introduced in that paper. After the present paper was submitted in mid May 2006, we learned about the papers [Hol, SJ] on so-called "rapid diffusion." Holt and coworkers describe experimental data on rapid diffusion through sub-2-nanometer carbon nanotubes with transport rates, for a range of gases, one to two orders of magnitude larger than would be predicted by assuming a Knudsen description of collisions. In other words, they show that the constant  $\xi$  can be quite big. The fascinating results they obtain may be a step toward developing efficient technologies for separation of gases: purifying  $O_2$  and  $N_2$  from air, separating  $CO_2$  from power plant flue gases, etc. The central concern of our paper is, in effect, to understand how  $\xi$ , which will be referred to as the *smoothness constant*, depends on the micro-geometry and in particular, how big a value it can attain. For example, a result described in section 1.5.2 shows that for a particular but typical surface microgeometry the smoothness constant is proportional to  $1 + A/R$ , where  $A$  is the gas molecule radius and  $R$  is a characteristic radius of the surface micro-geometry. (See section 1.5.2. The domain of validity of this approximate formula is described in section 2.2.) Although our initial motivation was more academic, we believe these recent results speak for the topicality of the basic question investigated here.

The structure of the present paper and its main results are described in the following subsections of this section. For the most part throughout the text the definition of a non-traditional symbol or term is in the same section, not

too far from where it is being used. When this is not the case, we indicate the subsection where the definition was given.

### 1.1 Time-of-escape experiment

The system described below is intended to model the Knudsen flow of gas in straight channels whose walls are characterized by some surface micro-structure, as in carbon nanotubes, for example. Thus our channels do not incorporate the traditional empirical concept of “tortuosity.”

Consider the following idealized experiment: a short pulse of inert gas is released from the middle point inside a 2-dimensional channel and the rate at which gas escapes the channel through the open ends is measured. There is no interaction among gas molecules, only between molecules and channel surface. The rate of escape determines the residence time, or *mean time of escape* from the channel. From the time of escape data, we wish to learn about the fine structure of the surface-gas interaction. By varying the channel length, thereby roughly controlling the number of collisions between surface and gas molecules, we expect to observe transport at different stages of development. This, in principle, provides a way to investigate how information about the surface fine structure is incorporated into the molecular motion through time.

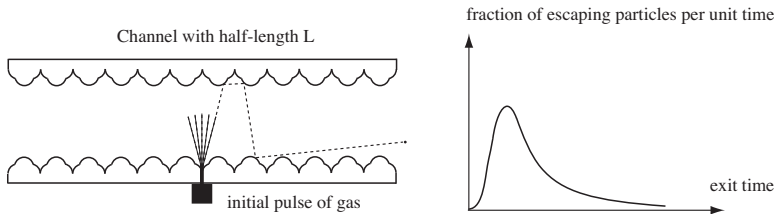


Figure 1: Idealized experiment measuring exit flow of a gas of billiard-ball molecules from a 2-dimensional channel. The periodic geometry lining the inner surface of the channel should be regarded as being much smaller in scale than the channel diameter, so that the time spent at a collision site is negligible compared to the time of free flight from one side of the channel to the other.

It is not too important for our study the precise place from which the pulse is released. One can imagine different configurations, such as injecting gas from one end that is subsequently kept closed, or injecting it from one end and measuring flow of gas through both ends. We chose the configuration of figure 1 for simplicity sake.

If the channel is short compared to its diameter, the number of gas-surface collisions is relatively small and we cannot take for granted that transport is well described by standard Fickian diffusion. For relatively short channel lengths our idealized experiment is akin to a (multi-) scattering experiment (in which time, rather than angle, is the observed quantity), whereas for relatively long

channel lengths what is measured is more characteristic of Fickian diffusion. Thus the experiment looks at different stages of gas flow by varying the channel length. To account for this dependence on channel length we introduce shortly the *diffusivity function*, which gives the effective diffusivity for varying lengths. This function converges to an ordinary diffusion constant as the length of the channel increases.

This *time-of-escape* experiment is inspired by experiments performed using TAP- and TAP-like systems [GYPS, Ni, Del1, Del2, WCM, W]. A concrete physical system that corresponds to our idealized experiment is, for example, the flow of gas through a long and straight carbon nanotube of large diameter compared to the size of the gas molecules, or through a narrow slit bound by (macroscopically) flat parallel surfaces.

Data from the time-of-escape experiment will be encoded in the *time-of-escape function*  $f(x)$  to be defined shortly (section 1.3), where  $x$  is the ratio of channel length over channel diameter. The central problem of the paper is how to extract transport properties, such as diffusivity, from this function. We are, for now, mostly concerned with asymptotic values of  $f(x)$  for large  $x$ , although this function should contain useful information also for small  $x$ .

The next subsection explains the gas-surface interaction model used in this paper.

## 1.2 The random-billiard model

We assume that individual gas-surface collisions follow the standard hard-spheres model as in [ACM], for example. Therefore, the scattering properties of these collisions are determined only by geometric features of the solid surface and the gas molecules. In [FY] we show how these features can be encoded in a scattering operator, which specifies the probabilistic profile of post-collisions angles. The simplest assumption to make about the surface geometry is that it is periodic. More complicated types of geometries can also be considered, but we restrict the present analysis to this simple case. (One can think of such regular geometries as simplified models of atomically smooth surfaces, or of ordered nanocluster arrays as in [Som], fabricated using electron beam technology.) This leads to the random-billiard model of gas-surface interaction introduced in [FY], whose main features we review below. One may think of this system as a model for gas transport in a slit channel whose parallel walls are described by planes (lines in dimension 2) that are macroscopically flat but have a regular lattice structure at the microscopic scale.

Here are some more details and terminology. Gas transport takes place in a cylindrical channel whose inner surface is lined with a periodic *micro-geometry* (see Figure 2). The channel can be of dimension 2 or 3, but in the present paper we restrict attention to dimension 2. A single period of the micro-geometry is called a *billiard cell*. The shape of a billiard cell is, in this model, the only characteristic property of the surface. (The billiard cell of Figure 2 is arbitrary. Several different examples will be considered in the course of this paper.)

Molecules are taken to be spherical. By following the trajectory of their

center of mass, and by “thickening” the billiard cell by an amount equal to the molecular radius, it can be assumed without any loss of generality that molecules are point-like. Therefore, the concept of microgeometry refers to the combination of the intrinsic geometry of the surface and the size (radius) of the probing gas molecules.

We assume a billiard-type (hard-spheres) dynamic inside the billiard cell, with uniform motion between collisions. In particular, the scalar velocity,  $v$ , of a gas molecule remains constant.

In kinetic theory of gases, the term “mean free path” refers to the trajectory between two consecutive collisions among gas molecules. In the Knudsen regime, this length is assumed to be large compared to the geometric dimensions of the channel (ideally infinite) so it makes sense to use the term to refer to the path between two consecutive collisions with the channel walls. We use  $\Lambda$  for the mean free path understood in this latter sense. Usually  $\Lambda$  is identified with the channel diameter. In our theory we distinguish two mean free paths: this same  $\Lambda$  and another, denoted  $\lambda$ , for the motion inside a billiard cell. Clearly, one typically has  $\Lambda \gg \lambda$ .

Figure 2 shows a molecular trajectory at two length scales: the microscopic, represented by  $\lambda$ , which has the order of magnitude of the cell’s width; and the macroscopic scale, represented by some characteristic length  $\Lambda$  of the channel, such as its diameter. When  $\Lambda/\lambda$  is big, we view the 2-dimensional channel as simply a pair of parallel straight lines. We then speak of *macro-collisions* between molecule and the channel surface, and the *micro-collisions* taking place inside the billiard cell. At the scale  $\lambda$  the motion is assumed to be deterministic but as shown in [FY] macro-collisions should be regarded as probabilistic. The post-collision direction is a random function of the pre-collision direction given by a Markov (scattering) operator,  $P$ , whose properties are summarized in section 4.

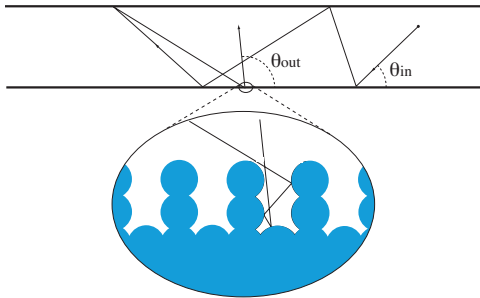


Figure 2: Channel with periodic microgeometry. A single period will be called a *billiard cell*. (The choice of geometry in this figure is arbitrary.) The two angles shown in the figure are the pre- and post-collision angles for  $P^5$ . (See text.)

The assumption of separation of scales, i.e., that  $\Lambda/\lambda$  is big, added to the

standard hard spheres model of collision lets us turn a somewhat complicated deterministic system into a Markov process that is both more amenable to detailed analysis and still reflects very closely the properties of the original system. Although the precise justification given in [FY] for this transition from the deterministic to the stochastic invokes passage to a limit  $\Lambda/\lambda \rightarrow \infty$ , the resulting stochastic model in itself does not depend on any assumption about this scale ratio. The random billiard can still be a useful model for molecular motion even when both  $\Lambda$  and  $\lambda$  are in the range of molecular size. For example, this model could be the basis of a theoretical analysis of inert gas flow in carbon nanotubes with diameter in nanometer range.

The mean number of micro-collisions at each macro-collision, the mean duration of a macro-collision, and the mean time of free flight inside billiard cells will be written, respectively,  $\langle N \rangle$ ,  $\langle t \rangle$ , and  $\langle s \rangle$ . The precise definitions are given in section 3. We call  $\langle t \rangle$  the *mean delay* at macro-collisions.

In principle, the structure of the surface can be defined by a hierarchy of micro-geometries with characteristic lengths  $\lambda_1 > \lambda_2 > \dots$ , where the  $\lambda_i$  can be taken as the mean free path of a point particle at the respective scale, each  $\lambda_i$  being much smaller than  $\lambda_{i-1}$  (see [FY]). An illustration of a micro-geometry with two scales is given in section 2.4. However, for the most part in this paper, surfaces will have a single micro-geometric scale  $\lambda$ . It should be noted that at all scales we have ordinary (non-fractal) geometry.

At the macro-scale, gas molecules follow a random flight between a pair parallel lines representing the channel in dimension 2. After each macro-collision, the particle direction is specified by the scattering operator  $P$  that gives the transition probability density of the macro-collision event  $\theta_{\text{in}} \rightarrow \theta_{\text{out}}$ , where  $\theta_{\text{in}}$  is the angle of pre-collision direction and  $\theta_{\text{out}}$  of post-collision direction. Transition probabilities after more than one macro-collision are given by iterates, or powers, of  $P$ . For example, the event  $\theta_{\text{in}} \rightarrow \theta_{\text{out}}$  depicted in figure 2 involves 5 collisions, and is described by  $P^5$ . The operator  $P$  contains the totality of information about gas-surface interaction properties that may influence transport. This information can, in principle, be extracted from scattering experiments.

In our previous paper, [FY], we investigated the asymptotic behavior of  $P^n$  for large  $n$  and showed how the so-called Knudsen cosine law can be understood as a stationary distribution of directions for  $P$ . Stated in a form that will be needed later in this paper, our interpretation of Knudsen's law is as follows. Let  $P_\mu$  represent the scattering operator that gives the Knudsen post-collision distribution of angles (represented by  $\mu$  in this paper) for arbitrary pre-collision directions. Then, independent of the choice of  $P$  amongst operators associated with random billiards,  $P^n$  converges to  $P_\mu$  as the number  $n$  of macro-collisions increases. (See section 4 for the proper definition of  $P_\mu$  and precise description of results.) That paper shows, in particular, that surface "roughness" is a *necessary condition* for the validity of Knudsen's cosine law. In the present paper we also see that the rate of convergence to  $P_\mu$  is a signature of the micro-geometry that strongly influences diffusivity. This leads to some explicit relations between the coefficient of diffusivity and micro-geometric parameters shown later in the paper.

### 1.2.1 Angle distribution versus delay at macro-collisions

Our results give a general conceptual mechanism for explaining how surface micro-geometry influences transport. There are at least two ways in which geometric properties of the surface can affect diffusivity. We call them *mean delay effect* and *angle distribution effect*.

The mean delay effect is due to the possibility that single macro-collisions may occur over a relatively long time span, as it may comprise a large number of micro-collisions; there is, in fact, no upper limit to how much time a molecule will spend in a billiard-cell. To understand how important the delay effect is, it is necessary to estimate the value of the mean delay  $\langle t \rangle$  in terms of geometric quantities. A precise value for  $\langle t \rangle$  is given as follows. Let  $A_b$  be the total area occupied by the billiard cells,  $A_c$  the total area of the channel,  $t_c$  the mean time between consecutive macro-collisions, excluding the time spent in billiard cells, and  $t_b = \langle t \rangle$  as defined above. The mean total time between consecutive macro-collisions is  $t_{\text{total}} = t_b + t_c$ . We show in section 3 that  $t_b/t_c = 2A_b/A_c$ . This gives a correction of the diffusivity constant by the multiplicative term  $A_c/(2A_b + A_c)$ . When  $A_c \gg A_b$  ( $A_c$  is proportional to the radius of the channel and  $A_b$  is roughly proportional to the size of the microscopic billiard cell), this correction term can be ignored. This holds under the separation of scales assumption.

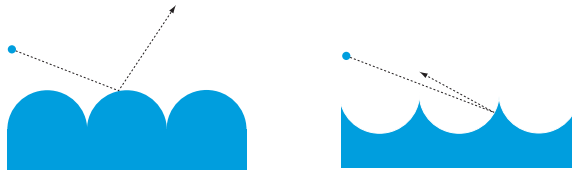


Figure 3: The Knudsen cosine law is not achieved in a single collision; the directions of pre- and post-collision motion are generally correlated. The exponential rate of decay of correlation is a signature of the micro-geometry reflected in the diffusivity constant. The picture on the left-hand side gives what is probably the more typical situation, in which these directions are positively correlated, implying faster diffusional transport than would be the case under the ideal Knudsen scattering law.

The angle distribution effect refers to how deviations from the Knudsen cosine law modify the mean free path in the channel. This has a strong influence on diffusivity, but it is often neglected in the literature, as it is usually assumed that the post-collision distribution of directions is exactly governed by the Knudsen law. We show in [FY] that the cosine law is the *stationary* distribution of directions but it is not generally achieved after a single collision. At any given moment during the motion of a gas molecule, memory of the present direction does not disappear at once. The angles after successive collisions have a degree of correlation (see figure 3) that decays exponentially with time. This exponential rate of relaxation towards the cosine law is a key signature of the

micro-geometry and has a strong influence on gas diffusivity. If the surface is very “smooth,” the molecule will move (back or forth) a longer distance on average, during a small interval of time, than it would on a more “rough” surface since it will tend to continue along the same overall direction for a little longer before the scattered angles become sufficiently randomized. (This happens, of course, throughout molecular motion, not only at the beginning; it does not matter how many collisions have already taken place since gas was released into the channel.) If the channel surface is very “rough,” this relaxation time is short, and the distance traveled during the same time interval will be smaller, resulting in lower diffusivity. This qualitative mechanism is explored quantitatively later in the paper. It suggests the following prediction for the typical effect of micro-geometry on diffusivity: to the extent that positive correlation of pre- and post-collision directions may be considered more typical than negative correlation (as in the left-hand side of figure 3) we should expect the diffusivity constant of most micro-geometries to be higher than the diffusivity for ideal Knudsen scattering.

### 1.3 Description of the time-of-escape function $f(x)$

Consider the quantity  $\tau(L, r, v)$ , defined as the mean time of escape of a pulse of gas released from the middle point of a channel of length  $2L$  and radius  $r$ , where  $v$  is the scalar velocity of the gas, assumed equal for all particles. As further explained below, we will for now disregard any thermal effects. If we wish to incorporate the temperature of the source into the analysis all that is needed is to assume that  $v$  is a random variable with standard Maxwellian distribution. On the other hand, we are assuming that the scalar velocity of the gas molecules is not changed by collisions with the channel wall, so the temperature of the channel itself does not enter into the present analysis.

It is convenient to work with a dimensionless quantity  $f(x)$ , where  $x = L/r$ , which is related to  $\tau$  by

$$\tau(L, r, v) = \frac{r}{v} f(x).$$

That  $\tau$  indeed has such a functional form is due to the elementary observation that for any positive number  $c$ , the mean time of escape satisfies the relations  $\tau(cL, cr, cv) = \tau(L, r, v)$  and  $\tau(L, r, cv) = \tau(L, r, v)/c$ .

Notice that  $f(x)$  depends exclusively on the micro-geometry specified in the model; any analytical or approximate expression obtained for  $f(x)$  will yield information about that geometry. Of course, geometric information is encoded in  $f(x)$  in a complicated way that cannot easily be extracted or described very explicitly, although we can gain a general understanding of the geometric content in  $f(x)$  by looking into specific families of micro-geometries as will be shown throughout the paper. The next subsection gives a “toy” example.

### 1.3.1 A simple example: the “hair comb” micro-geometry

A simple example will help explain the way in which the time-of-escape function  $f(x)$  is related to both the geometry of the random-billiard and gas diffusivity. First, consider the hair-comb micro-geometry of figure 4.

For concreteness, let us suppose that the initial direction is given by the angle  $\theta = \pi/4$  and the lengths of the base,  $b$ , and height,  $h$ , of the rectangular cell satisfy  $b > 2h$ . (Expression 1 takes a different, much more complicated, form if no restrictions are imposed on  $b$ ,  $h$  and  $\theta$ .) Gas molecules are assumed point-like. It can be shown that, for large values of  $x$  (i.e., large ratio  $L/r$ ) the asymptotic expression holds:

$$\frac{f(x)}{x^2} \sim \frac{1}{\sqrt{2}} \left( \frac{b}{2h} - 1 \right)^{-1}. \quad (1)$$

Therefore, the single geometric parameter of the hair-comb family, namely the ratio  $b/h$ , can be recovered from the function  $f(x)$ . This follows from a central limit theorem for Markov chains (see [Fe]), which can also be used to show that for long channels the gas concentration  $u(t, z)$ , as a function of time and space coordinates along the channel axis, satisfies a standard diffusion equation

$$\frac{\partial u}{\partial t} = D \frac{\partial^2 u}{\partial z^2},$$

where  $D = (1/\sqrt{2})(b/2h - 1)rv$  is the gas diffusivity,  $r$  is the channel radius, and  $v$  is the constant scalar velocity of the gas molecules.

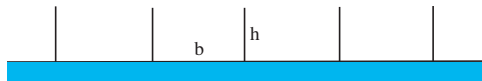


Figure 4: The hair-comb micro-geometry.

## 1.4 The smoothness and diffusivity functions

The diffusivity constant in the Knudsen regime is often written as  $D = \xi D_0$ , where  $D_0$  is a theoretical value derived in the kinetic theory of gases and  $\xi$  is an empirical correction term. We introduce in this section a function  $\xi(x)$ , the *smoothness function* of the normalized channel length,  $x = L/r$ , and a notion of effective diffusivity also depending on  $x$ .

Before giving the precise definition of these functions, it will be helpful to make a few remarks of a probabilistic nature. The concentration,  $\phi(z, t)$ , of a large number of particles undergoing independent Brownian motion in dimension one is governed by the equation

$$\frac{\partial \phi}{\partial t} = D \frac{\partial^2 \phi}{\partial z^2}. \quad (2)$$

Let  $B_t$  represent the position along the  $z$ -axis of a single Brownian particle that started at position  $z = 0$  at time  $t = 0$ . If  $\tau(L)$  is the mean time it takes  $B_t$  to be at a distance  $L$  from the origin, then it can be shown that  $L = \sqrt{2D\tau}$ , or

$$D = L^2/2\tau(L). \quad (3)$$

Suppose now that the random motion of the individual independent particles is given not by continuous Brownian motion, but by a sequence of small random flights having mean time  $\bar{t}$  and mean square displacement  $\delta^2$ . It follows from the standard central limit theorem that for times  $t \gg \bar{t}$ , the concentration  $\phi(z, t)$  is still governed by the same equation 2, were  $D = \delta^2/\bar{t}$ , while 3 must be replaced with

$$D = \lim_{L \rightarrow \infty} L^2/2\tau(L). \quad (4)$$

Equation 4 is ideally suited for our purposes since it expresses the diffusivity constant in terms of quantities that are directly measured in the time-of-escape experiment. An example of how this relates to the micro-geometry of a random billiard was given above in subsection 1.3.1.

There is, however, a difficulty in using expression 4 for random billiards with more typical micro-geometries than that of 1.3.1. For a two-dimensional channel, under the assumption that the Knudsen cosine law holds either exactly or asymptotically, the mean square displacement along the channel between consecutive macro-collisions is not finite (see, e.g., [BGT]), which can be shown by an elementary geometric argument. In this case  $\delta^2 = \infty$  and  $\bar{t} < \infty$ , and the standard central limit theorem does not hold. It is shown in [BGT] that the random flight under the Knudsen cosine law still leads to ordinary Brownian motion and that equation 2 still holds after an appropriate re-scaling of time. This re-scaling amounts to introducing a logarithmic term in the expression for  $D$ :

$$D = \lim_{L \rightarrow \infty} \frac{L^2}{2\tau(L, r, v) \ln(L/r)}, \quad (5)$$

where  $r$  is the channel radius and  $v$  is the scalar velocity of the gas molecules. For three-dimensional channels and non-zero channel temperature the logarithmic term disappears, as is well-known from classical kinetic theory of gases. (It also disappears if the channel is not perfectly straight, so that the mean free path becomes finite. This is an argument used in [ACM], where a cutoff parameter  $\epsilon$  is introduced in order to bypass the same difficulty.) So it is not clear how physically meaningful this term really is. It must, nevertheless, be incorporated into the expression of  $D$  if we want to avoid adding to our basic model further *ad hoc* assumptions. The essential point is that if  $L \gg r$  the diffusion equation 2 still holds, with  $D \sim L^2/(2\tau \ln(L/r))$ , whenever the stationary distribution of angles for the two-dimensional random flight is given by Knudsen cosine law.

This suggests introducing a function  $D(L, r, v)$  that gives the effective diffusivity for a given channel length:

$$D(L, r, v) = \frac{L^2}{2\tau(L, r, v) \ln(L/r)}. \quad (6)$$

Written in terms of the dimensionless time-of-escape function  $f(x)$  the effective diffusivity is  $D(L, r, v) = rv\mathcal{D}(x)$ , where  $x = L/r$  and  $\mathcal{D}(x)$  is a dimensionless function given by

$$\mathcal{D}(x) = \frac{x^2}{2f(x)\ln x}. \quad (7)$$

(Notice the change in font. We designate the dimensionless counterpart of a dimensional quantity by the same letter in calligraphic font. Thus  $D$  and  $\mathcal{D}$ ,  $D_0$  and  $\mathcal{D}_0$ .)

We define the *smoothness function*  $\xi(x)$  of a given micro-geometry as the ratio

$$\xi(x) = \mathcal{D}(x)/\mathcal{D}_0(x) = f_0(x)/f(x) \quad (8)$$

where  $\mathcal{D}_0(x)$  is the diffusivity function and  $f_0(x)$  is the time-of-escape function under *ideal roughness* conditions. A surface with ideal roughness is defined as one for which the Knudsen cosine law is exactly valid at every collision rather than valid only in the asymptotic sense. It should be noted that what we are calling “ideal roughness” does not amount to “maximal roughness,” as will be seen later in the paper when discussing the effect of sharp tip angles and cusps. The diffusivity function under ideal roughness, and the associated dimensionless diffusivity function, are related by  $D_0(L, r, v) = rv\mathcal{D}_0(x)$ .

The limit of  $\xi(x)$  for large  $x$ , denoted  $\xi$ , will be called the *smoothness constant*. This is a purely geometric quantity associated to the micro-geometry. The idea that large values of  $\xi$  are associated with high degree of surface “smoothness,” or “flatness,” understood in the ordinary geometric sense of these terms, will be explained later in the paper by means of both analytical and numerical examples. It will also be seen that  $\xi$  can achieve arbitrarily large values by making the geometry sufficiently flat. (In particular, it does not make sense to speak of Fickian diffusivity under “ideal smoothness” conditions.)

We can now express the diffusivity constant of equation 2 as

$$D = \mathcal{D}_0\xi rv, \quad (9)$$

where  $\xi$  is the smoothness constant and  $\mathcal{D}_0$ , defined as the limit of  $\mathcal{D}_0(x)$  for large  $x$ , is a dimensionless constant independent of surface or gas properties whose value we do not attempt to determine here.

Since in the hard spheres collision model the scalar velocity  $v$  does not change during molecular motion,  $v$  only depends on the temperature of the initial pulse of gas according to the expression  $v = A_m\sqrt{T/M}$ , where  $A_m$  is the molecular radius and  $M$  is the molecular mass. Other things being equal, the bigger the value of the smoothness constant  $\xi$ , the faster diffusional transport will be, as equation 9 makes clear.

The coefficient  $\xi$  is traditionally termed “roughness” in the literature, but we prefer to call it “smoothness” since, as will be seen here, it increases with the degree of surface smoothness, or flatness, understood in the naive geometric sense. It is more natural to speak of transport being facilitated by greater surface smoothness, not by greater roughness.

### 1.4.1 A coin model of gas transport

A rather simplified probabilistic model of transport can help to identify and interpret some features of the random billiard model that will be seen later. We call this the *coin model* of gas-surface interaction. This will, in particular, help interpret the concept of smoothness just introduced.

Fix a number  $\alpha$  between 0 and 1, which will be referred to as the surface *slippage*. Molecular motion is represented by a random walk on a one-dimensional lattice with spacing  $\delta$  between neighbor cells. A molecule moves by jumping one step of length  $\delta$  either backward or forward, the time between jumps being given by a constant  $\bar{t}$ . The direction of jump is decided by the following rule: at each step we flip two coins simultaneously, one biased, with probability for heads equal to  $\alpha$ , and the other unbiased. If the biased coin comes up heads the molecule repeats the behavior of the previous jump regardless of the outcome of the unbiased coin. We say in this case that the molecule *slips* with probability  $\alpha$ . If the biased coin comes tails the molecule *forgets* what it did in the previous jump and moves forward or backward depending on the outcome of the unbiased coin (say, heads = forward, tails = backward.)

There are only two directions of motion, represented by  $\pm 1$ . The scattering operator  $P$  for this example is the transition probabilities matrix

$$P = \begin{pmatrix} \frac{1+\alpha}{2} & \frac{1-\alpha}{2} \\ \frac{1-\alpha}{2} & \frac{1+\alpha}{2} \end{pmatrix}$$

The top-left entry,  $(1 + \alpha)/2$ , is the probability that the particle direction in the next move is  $+1$  given that it was  $+1$  in the last move; the lower-left entry,  $(1 - \alpha)/2$ , is the probability that the next direction is  $+1$  given that in the last move it was  $-1$ , etc. Zero slippage corresponds to ordinary random walk on a one-dimensional lattice, in which no memory of past moves is kept. The case  $\alpha = 1$  corresponds to purely deterministic uniform motion forward or backward.

The Markov chain specified by  $P$  has the same unique stationary distribution of directions for all  $\alpha \neq 1$ , namely, probability  $1/2$  for both  $+1$  and  $-1$ . Transport, however, proceeds at different speeds depending on  $\alpha$ . More precisely, let  $D_\alpha$  denote the diffusivity for the process given as a limit of this random walk, by making  $\delta$  and  $\bar{t}$  go to 0 so that the ratio  $D_0 = \delta^2/\bar{t}$  remains constant. Then it can be shown, using the central limit theorem for Markov chains, that

$$D_\alpha = \frac{1 + \alpha}{1 - \alpha} D_0.$$

The quantity  $\xi_\alpha = (1 + \alpha)/(1 - \alpha)$  should be compared with the smoothness constant (limit of the smoothness function) introduced above. (Notice that  $\eta = 1 - \alpha$  plays the role of the Smoluchowski diffusivity coefficient mentioned at the beginning of section 1.) The reference diffusivity,  $D_0$ , in this example is associated with standard random walk, whereas in the definition given earlier we used the dimensionless diffusivity  $\mathcal{D}_0$  for ideal Knudsen scattering. Nevertheless, the same expression of  $\alpha$  will be seen later for the smoothness of certain choices of micro-geometries. (See section 3.3.) One can also introduce a diffusivity

function for the coin model by taking a one-dimensional lattice interval of finite but variable length and measuring the hitting time at the ends of the interval. The definition is essentially the same as above, but without the logarithmic term.

We emphasize the following property of this random walk example: the stationary distribution of directions, which corresponds to the Knudsen cosine law for more realistic gas-surface collision models, does not change as we vary  $\alpha$ , but the speed of convergence to the stationary distribution varies greatly with slippage. In fact, it can be shown that the number of steps (collisions) before an initial distribution of directions becomes close to the stationary distribution is proportional to  $1/(1 - \alpha)$ . Therefore, as  $\alpha$  is close to 1 (high slippage), it will take longer to reach stationarity. The diffusivity constant will be proportionally larger as particles effectively move a greater distance on average during a small interval of time. It is sometimes possible to associate a value of  $\alpha$  to a micro-geometry in the random billiard model, as will be seen later (e.g., in subsection 2.4). When this can be done, it makes sense to say that flatter surfaces promote faster diffusional transport by being more “slippery.” It should be possible to obtain a general definition of slippage in terms of the operator  $P$  of a random billiard based on some measure of the statistical correlation between pre- and post-collision angles, although we have not pursued this idea in this paper.

## 1.5 Influence of microgeometry on diffusivity

Our, mostly numerical, study of how micro-geometry affects transport is described in section 3. We give here an overview of the main results, indicating the subsections of section 3 where each topic is developed in greater detail.

We consider several parametrized families of micro-geometries and study properties of the gas transport by numerical simulation of the time-of-escape experiment. Each family is designed to explore the effect on diffusivity of a different geometric feature.

### 1.5.1 Main geometric features

First, we need to introduce some vocabulary to describe the micro-geometric features of interest.

The assumption that macro and micro scales are far apart imply that the only geometric features of interest are those which are invariant under homothety (i.e., properties left unchanged under dilations or contractions). Examples are angles and length ratios. A natural reference scale for the micro-geometry is the length of the open side, or *period*, of the billiard cell (this is  $e$  in figure 5). So, for example, the radius  $R$  (figure 5) would not appear by itself in, say, the smoothness function of this micro-geometry, but the ratio  $R/e$  is a valid geometric feature.

A point of maximal height for the micro-geometry will be referred to as a *tip point*. (This is the point  $p$  of figure 5.) We refer to the region around tip points as the *exposed* part of the surface (or micro-geometry) and the rest of the surface

as the *shadowed* part. (In figure 5, the exposed part lies above the dashed line close to  $p$ .) Even without specifying the exact size of the neighborhood of  $p$  comprising the exposed part, the concept is useful for explaining the main observation of section 2.3: the part of the micro-geometry that affects diffusivity most strongly is very narrowly concentrated around tip points. The notion of exposed side is, thus, a way to focus attention on the part of the geometry having strongest effect on gas transport properties. The features of the exposed side to be studied in detail are: the (normalized) radius of curvature,  $\rho$ , (for the example of figure 5,  $\rho = R/e$ ), the *tip angle* (this is the angle  $\eta$  of figure 5) and *flat tops* (same figure). The latter can be expressed as the ratio  $d/e$ , where  $e$  refers to the period of the geometry shown at the bottom right side of the figure.

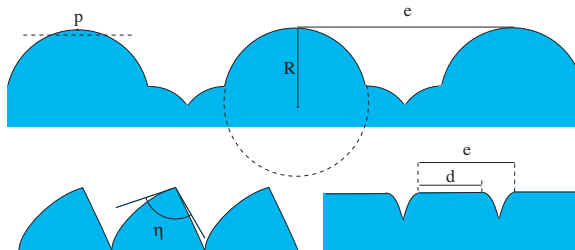


Figure 5: Definition of some of the geometric features of a micro-geometry: tip point,  $p$ , exposed part (region near  $p$  above dashed line), length of open side  $e$ , normalized radius  $\rho = R/e$  of exposed part, tip angle  $\eta$ , and flat exposed part. A tip point is called a *cuspl* if  $\eta = 0$ . We may occasionally refer to  $e$  as the *period* of the micro-geometry.

In subsection 2.3 we investigate what we call the *shadowing* effect. This refers to the observation that the exposed part of the micro-geometry affecting diffusivity is a small fraction of the total surface area. It is not possible on the basis of numerical calculations alone to know exactly how small the exposed part is, but our results are consistent with the possibility that only features at the tip point influence diffusivity, such as normalized radius of curvature and tip angles.

### 1.5.2 Relationships between microgeometry and diffusivity

The observed dependence of diffusivity on the normalized radius  $\rho$  has a fairly regular and monotone form. The simplest geometry used for studying this dependence is shown in figure 6. We first recall that the micro-geometry of the channel inner surface should be understood as the effective geometry seen by the center of mass of gas molecules. With this in mind, let  $A$  denote the molecular radius. If the actual geometric profile of the surface is the shaded area of Figure 6, then for different values of  $A$  the microgeometry is represented by the circular lines with radius  $R + A$ . In this case,  $e = 2R$ , so  $\rho = (R + A)/2R = (1 + a)/2$ ,

where  $a = A/R$ . (We will use the parameter  $1 + a$  rather than  $\rho$  at several places later.)

The numerical results shown later suggest the approximate expression for smoothness as a function of  $\rho$  (see section 2 for a discussion about errors and range of validity of this expression):

$$\mathcal{D}_\rho/\mathcal{D}_0 = 2.6\rho. \quad (10)$$

Relation 10 can in principle be used for primary estimates of geometric properties of real surfaces. For example, a highly polished surface may be viewed as having a higher average value of  $\rho$  than “rough” surfaces. If this is the case, we should expect to be able to detect surface roughness by a measurement of diffusivity. Notice that, since  $\rho$  approaches  $A/(2R)$  for large  $A$  compared to  $R$ , and to  $1/2$  for small  $A$ , then  $1.3 < \mathcal{D}_\rho/\mathcal{D}_0 < 1.3A/R$ . Although this was obtained for the specific micro-geometry family of figure 6, the simple dependence  $\mathcal{D}_\rho/\mathcal{D}_0 \propto \rho$ , may be typical of surfaces without sharp corners at the scale of the gas molecule radius. This suggests that small value of smoothness (compared to 1) may indicate some feature not present in this *bump family*, such as sharp tips and edges on the exposed side. (More on this later.)

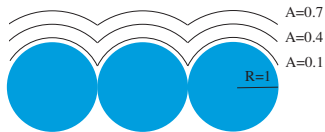


Figure 6: Microgeometries parametrized by the radius,  $A$ , of the probing gas molecules. The indicated values will be explored numerically in section 2.

Taking this simplified two-dimensional model as a very rough guide, consider for example the case of atomically smooth carbon pores [Hol, SJ] and argon as probe molecules. In this case  $R = 0.77 \times 10^{-10}m$  (carbon)  $A = 0.98 \times 10^{-10}m$  (argon), so  $\xi = 1.3(1 + 0.98/0.77) = 2.95$ . Since this value was obtained using a hard spheres model of interaction, it should likely be taken as an underestimation of  $\xi$ . Heuristically, “softening” the physical interaction increases smoothness. Whether  $\xi$  increases enough to explain the experimental data of [Hol, SJ] will require further study.

If two surfaces have average values  $\rho_1$  and  $\rho_2$  for the normalized radius when probed by gases with molecular radius  $A$ , then the ratio of their coefficients of diffusivity is approximately

$$\mathcal{D}_{\rho_1}/\mathcal{D}_{\rho_2} = \frac{1 + (R_1/A)}{1 + (R_2/A)}.$$

If, on the other hand, a surface is probed with gas molecules of radii  $A_1$  and  $A_2$ , then

$$\mathcal{D}_{\rho_1}/\mathcal{D}_{\rho_2} = \frac{1 + (A_1/R)}{1 + (A_2/R)}.$$

Qualitatively, the effect of  $\rho$  on diffusivity for the bump family is captured by figure 7. Due to the shadowing effect, this dependence on  $\rho$  should be valid for more general geometries having the same kind of exposed side.

To understand the effect of a flat exposed side (subsection 2.4) we use both numerical and analytical calculations. The results are consistent with the following approximate expression for the smoothness constant:

$$\mathcal{D}_\alpha/\mathcal{D}_0 = \frac{1 + \alpha}{1 - \alpha},$$

where  $\alpha = d/e$ . Thus it is natural to assign a value of slippage,  $\alpha$  (as in the coin model), to this kind of micro-geometry. We indicate later how a value of slippage can be assigned to micro-geometries whose main geometric feature is the normalized radius  $\rho$ . This expresses  $\alpha$  in terms of  $\rho$  for the micro-geometry of figure 6. (Recall that  $1 - \alpha$  corresponds, in the Maxwell-Smolukowski model, to the fraction of diffuse collisions.)



Figure 7: The top geometry, with bigger curvature, produces slower diffusion than the one at the bottom.

There are other geometric features of surfaces that can in principle be detected by measurements of the coefficient of diffusivity, such as tip angles and cusps. The dependence of diffusivity on tip angle also shows a fairly regular monotone behavior. This is described in detail in subsection 2.5. We only make here the following qualitative observation. It is natural to ask how low the smoothness ratio  $\mathcal{D}/\mathcal{D}_0$  can be as we vary the micro-geometry. In all examples in which the tip point is not a corner (i.e., so that the surface has a unique tangent line at  $p$ ), smoothness is always greater than 1. However, we do have examples with  $\xi$  less than 1. Their common feature is that all have corners at the tip point. The smallest value of  $\xi$  is seen when the micro-geometry has a cusp.

The observation that smoothness can in principle be less than 1 may seem surprising in view of the Maxwell-Smoluchowski model of surface roughness. Recall that, in this model,  $\xi = (1 + \alpha)/(1 - \alpha)$ , where  $\alpha$  is the fraction of specular collisions. (We used  $\eta = 1 - \alpha$  at the beginning of section 1 for the fraction of diffuse collisions.) So  $\xi$  cannot be less than 1 and the Knudsen diffusivity is the smallest value the Smoluchowski diffusivity can attain. This is an indication that surface morphology enters into  $\xi$  in a more complicated way than this classical model would suggest.

## 1.6 Delay during a macro-collision

The time gas molecules spend at a macro-collision site (that is, inside a billiard cell) is sometimes assumed to be the main reason why rougher surfaces are expected to have smaller values of diffusional transport than smoother surfaces. It is, therefore, of interest to obtain a precise estimate for the amount of time spent in billiard cells.

There are at least two ways in which time spent in billiard cells, or the *delay* at a macro-collision, could affect transport. The first is that the delay can be arbitrarily large, even infinite; in other words, molecules that enter a cell at very particular angles and positions may get trapped in. (It can be shown that the micro-geometries of figure 10, for example, and many others, admit an infinite number of initial conditions leading to such trapped trajectories, although these trajectories constitute an event of zero probability.) Even disregarding trapping, there might be large enough delay on the whole to affect the value of diffusivity in a significant way.

Secondly, there could in principle be enough delay that incoming molecules might hit at a site that is temporarily occupied by another molecule. This would affect diffusivity not due to the delay itself, but by possibly creating a form of dynamic covering.

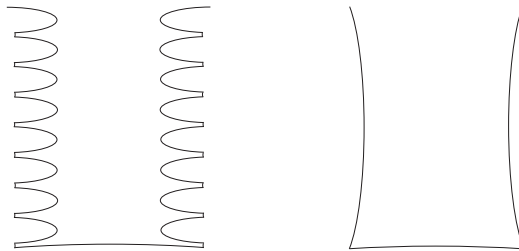


Figure 8: The average delay,  $\langle t \rangle$ , is nearly the same for the two geometries shown above, although the average number of micro-collisions,  $\langle N \rangle$ , is over three times greater for the cell on the left. As the number of bumps grows (assuming same height and same base),  $\langle t \rangle$  stays nearly constant while  $\langle N \rangle$  grows approximately linearly.

We show that these effects are easily estimated. More precisely, we show that the ratio of mean delay at macro-collisions over the mean time of free flight from one site to the next along the channel is equal to the ratio  $2A_b/A_c$ , where  $A_b$  is the total area occupied by the billiard cells and  $A_c$  is the total area of the channel. (A similar relation holds for volumes if the channel is 3-dimensional.) It follows that the effect that delay in billiard cells has on diffusivity will be negligible if  $A_b/A_c$  is sufficiently small. This is shown in section 3. Therefore, the assumption about separation between micro and macro scales in our model implies that trapping or long delay are not going to be a factor in diffusivity.

Let  $\langle N \rangle$  denote the average number of (micro) collisions taking place inside a billiard cell from the moment the gas molecule enters the cell till it leaves, count-

ing the arrival back to the open side, prior to leaving the cell, as one collision. Let  $\langle t \rangle$  be the delay as defined before. If  $l$  represents the cell's perimeter including the length,  $e$ , of the open side,  $A$  the area of the cell, and  $v$  the molecular scalar velocity, then these quantities are related by the exact expressions

$$\langle N \rangle = l/e, \quad \langle t \rangle = A\pi/ev. \quad (11)$$

A similar expression is shown in section 3 for the average time,  $\langle s \rangle$ , between consecutive micro-collisions.

The precise conditions and definition of averages (which must be taken with respect to the stationary measure  $\mu$ ) are described in section 3. These relations are illustrated there by calculations based on numerically simulating the molecular flight inside cells of varying shapes.

## 1.7 Thermal effects

We disregard in this paper any thermal effects. This is implicit in the hard-ball interaction model we have adopted. The domain of validity of this assumption (that is, understanding how quickly the fast moving gas molecules exchange energy with the solid surface as a function of the number of collisions) is a problem of special interest which is discussed, for example, in the papers [JBS, BJN], as well as [ACM] and references cited there. Since our random-billiard model assumes that the distribution of scalar velocities of the initial pulse is not altered during transport, only the temperature of the initial pulse of gas is significant here. This temperature can be incorporated into the expression of diffusivity in a simple-minded way (see equation 9). On the other hand, to incorporate the channel temperature into this model one needs to refine our definition of the scattering operator  $P$ . This is necessary in order to determine how easily (or in what range of temperatures) the geometric features studied here can be detected in an actual experiment. In other words, in this paper we are focusing on the determination of the purely geometric features that can influence diffusivity and leave for a future study the question of whether these geometric effects are sufficiently robust to reveal themselves above the randomizing action of lattice vibration. A more refined version of our random-billiard scattering operator that also models wall temperature will be considered in a future study. Our present gas-surface interaction model should be regarded as a low temperature limit of such a more general model.

## 2 Numerical determination of smoothness

For a precise theoretical understanding of how  $\xi(x)$  and  $\xi$  (see definitions in section 1) reflect the micro-geometry of the channel surface it will take, ultimately, a much more detailed probabilistic analysis than what we have done so far. Before further analysis can be attempted, one needs some preliminary insight into what geometric features may turn out to be most relevant and what approximate functional relations are involved. In this section we describe the

results of a series of numerical experiments devised to give such a preliminary understanding. The value of these experiments lies, in part, in the questions and conjectures they raise, which we hope will eventually be settled by further analytical study or more refined numerical work.

Most of the information we have obtained is summarized in the figures throughout the section. A quick inspection of these figures will tell what are the geometric features we explored and how robust or regular is the effect of each feature on  $\xi$ . In the body of the text we attempt to interpret some of this information. We have used at certain points expressions such as “it seems” or “it is apparent” to warn the reader when we think our interpretations are more tentative.

A typical figure (for example, 15) shows a family of graphs, each representing the smoothness function  $\xi(x)$  for different parameter values of a family of microgeometries. (In figure 15, for example, the family is shown next to the graphs of  $\xi(x)$ , but in other examples the family may be shown on a separate figure nearby.)

The next subsection gives some details on how the computations were performed and some of the numerical parameters involved. It is followed by mostly independent subsections that investigate different aspects of the micro-geometry.

We mostly concentrate on  $\xi(x)$  for relatively large values of  $x$ , although one should expect  $\xi(x)$  for small  $x$  to also contain interesting information. We only mention here that the nature of this function varies with the choice of micro-geometry, but it is not yet clear what determines, for example, whether  $\xi(x)$  is increasing or decreasing in  $x$ . In most examples this is an increasing function, but in the presence of sharp tip angles it can be initially decreasing. See the graphs in figure 15 and 18.

## 2.1 Overview of numerical approach

We briefly sketch here how the computations were performed. We wrote a program consisting of three parts: part 1 specifies the shape of the billiard cell and executes the (deterministic) billiard motion in it. For simplicity, cells were limited to contours composed of segments of circles and lines. In part 2, a matrix approximation of the scattering operator  $P$  is obtained by computing the billiard trajectory in the cell for a range of initial conditions. The angles  $\theta_{\text{in}}$  and  $\theta_{\text{out}}$  (see section 1.2) were sampled at intervals of size  $\pi/400$ . This gives a matrix approximation of  $P$  of size  $400 \times 400$ . For each initial angle  $\theta_{\text{in}}$ , the initial position  $x$  along the open side of the billiard cell (normalized to length 1) was sampled at intervals of size  $1/1000$ . The  $(i, j)$ -entry of the matrix is then determined by the fraction of these trajectories leaving the cell at an angle  $j\pi/400$  (having entered it at angle  $i\pi/400$ .) Using this approximation for  $P$ , part 3 now executes the experiment proper. For each fixed ratio  $x = L/r$  of channel length over channel diameter (recall that  $L$  is half of the channel length), the program obtains the random flight between the two parallel lines representing the walls of the channel, starting from the middle point of one of the lines until the trajectory leaves the channel at one of the two ends. The time of exit is

then registered. This is done 10000 times for each value of  $x$ . We refer to these 10000 random trajectories as representing a “pulse of gas” (of 10000 molecules). In figure 9 (top graph) or figure 10 each dot represents a single pulse. (In other graphs the dots are connected for the sake of better visualization.) The sample average then gives the estimated value for the dimensionless mean exit time  $f(x)$  defined in section 1.3. The length parameter  $x$  was sampled over the range 3 to 150 at steps of length 3. Part 3 is by far the most computationally intensive. Computer time for each pulse increases, roughly, with the square of  $x$ . This is the main limitation in extending the calculation to longer lengths. (With an ordinary personal computer running a general purpose mathematics software, it typically took between 2 and 3 hours to simulate a pulse for  $x = 150$ .) Another potential limitation associated to large values of  $x$  is that grazing angles are expected to become more important as  $x$  increases, so the step size used for sampling the angles may begin to introduce systematic errors at some point, although we have not detected such errors for the range of  $x$  we analyzed. Assuming no unexpected systematic errors, the statistical error in estimating  $f(x)$  by the sample means (shown on the graphs) was typically of the order of 5% or less of these means, for a 95% confidence interval. This accounts for the fluctuation observed for  $\xi(x)$  on the graphs.

Any mention in this section of the smoothness constant  $\xi$  really refers to the average of the last 10 sampled values of  $\xi(x)$ , that is, the values obtained for  $x = 123, 126, \dots, 150$ . We cannot at present determine how close this computed value is to the theoretical limit defining the constant  $\xi$ . In practice this may not be of much consequence since it is the value of  $\xi(x)$  (the effective smoothness at a given length) rather than the constant  $\xi$  (limit for  $x \rightarrow \infty$ ) that should be most relevant.

## 2.2 Curvature of exposed side

We investigate here the effect on smoothness of changing the normalized radius  $\rho$ . We do this for the family of geometries depicted in figure 6. (The notation used here is explained in subsection 1.5. Notice that we use below the normalized molecular radius  $a = A/R$  rather than  $\rho$  itself. Recall that  $\rho = (1 + a)/2$ .) The expected dependence of diffusivity on  $1 + a$  is described qualitatively in figure 7: small values of  $a$  (large bump curvature of the exposed part) correspond to slow diffusion.

Also recall that the smoothness function is  $\xi_a(x) = \mathcal{D}_a(x)/\mathcal{D}_0(x)$ . The graph of figure 9 gives  $\xi_a(x)$  for a range of values of  $a$ . The smoothness constant for each  $a$  is given by the value of the horizontal asymptote that each graph of Figure 9 seems to possess. Over the range of  $x$  explored,  $\xi_a$  can be approximated by the linear relation:

$$\xi_a = 1.3(1 + a).$$

The constant 1.3 was obtained by averaging  $(\mathcal{D}_a(x)/\mathcal{D}_0(x))/(1 + a)$  over the last 10 values of  $x$ , and over  $a$ , giving 1.27 with a standard error 0.06. It would be highly desirable to confirm this simple relation by either analytical means or

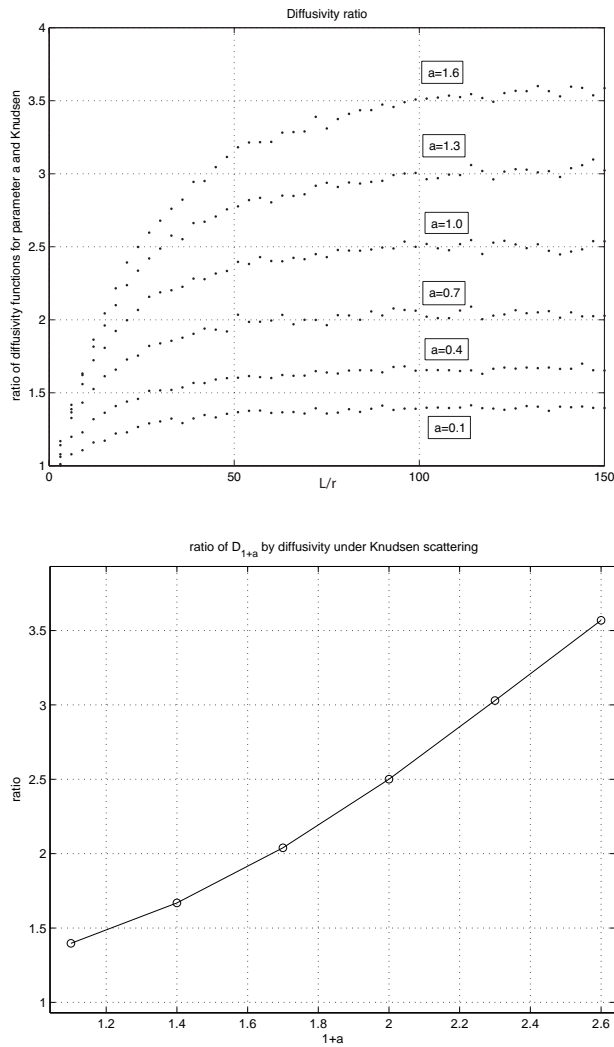


Figure 9: Above: the smoothness function,  $\mathcal{D}_a(x)/\mathcal{D}_0(x)$ , for a range of values of  $a$ . Below: smoothness constant as a function of  $1+a$ . Each dot in the family of graphs at the top corresponds to a pulse of  $10^4$  molecules. Here,  $x = L/r$ , and we take the average value of  $\xi(x)$  for  $x = 123, 126, \dots, 150$  as our approximation of the smoothness constant.

more refined numerical work than ours. The reader should refer to section 1.5.2 for further discussion of this formula.

### 2.3 Shadowing effect

The dependence of diffusivity on the parameter  $a$  was shown in the previous subsection for a simple geometry, with a single curved (circular) side. For more complicated geometries, one expects quite naturally that it is the curvature of the exposed side that influences the diffusion properties most strongly. What is perhaps surprising is how strongly and sharply this phenomenon, which we refer to as the *shadowing effect*, turns out to be, at least in dimension 2.

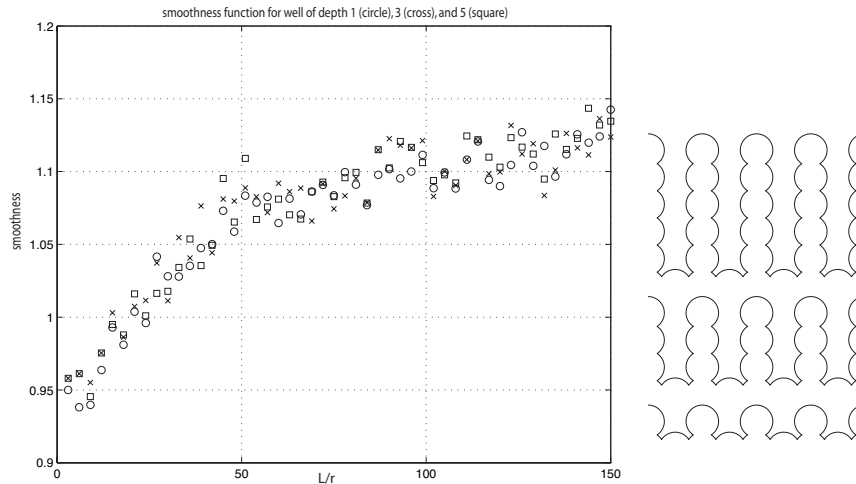


Figure 10: Values of smoothness as a function of the ratio  $s = L/r$  for the three well micro-geometries. Depth 1 is represented by circles, depth 3 by crosses, and depth 5 by squares.

In this section we give further evidence of this effect, without attempting at this point to provide a theoretical justification for it. We begin by considering the three similar micro-geometries shown on the right-hand side of figure 10. We refer to them as the *well* micro-geometries of depth 1, 3 and 5, respectively.

On account of the shadowing effect, we should expect relatively little difference in their smoothness functions. The precise values are as follows. The average values of  $\xi(x)$  over the last (largest) 10 values of  $x$  are (for depths 1, 3 and 5, in this order): 1.117, 1.116, and 1.122, all within a standard deviation of each other. (The standard deviation is  $1.3 \times 10^{-2}$  for all three.) The change in smoothness due to depth observed here can thus be attributed to statistical error. The graph of figure 10 shows the individual values of  $\xi(x)$  as a function of the normalized length  $x$ .

Something very different happens when changes are made to the exposed part of the geometry. Consider next the family of contours shown in Figure 11. We wish to compare the two geometries of the bottom pair and the two geometries of the top pair. The value of  $a$  of the large arcs is the same for the two geometries in each of the two pairs. For the top pair, the contour is changed in the middle region between the large arcs. For the bottom pair, a small bump is added at the top.

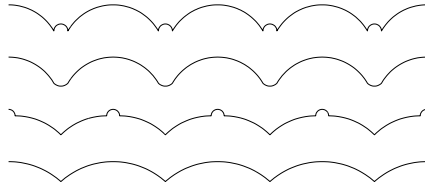


Figure 11: Comparison of two pairs of geometries. The added top bump (bottom pair) has a strong effect on diffusivity, but the change in the geometry of the shadowed part (top pair) has negligible effect.

The average of  $\xi(x)$  over the last 10 values of  $x$ , for each of these four geometries, is as follows. For the top and second to top (the first pair of geometries), this average is, respectively, 1.36 and 1.33, a change of approximately 2% over the smaller value, barely above what can be expected from chance alone (a little over 1%). (The parameter  $1 + a$  for the exposed side of the top two contours is 1.1.) The approximate value 1.3 of their smoothness constants is the one predicted by the lowest graph of figure 9. Therefore, the addition of the middle bump does not have any significant effect on diffusivity. On the other hand, for the third and fourth geometries from the top, the values are 1.05 and 1.78, a change of nearly 70% over the smaller value, well above statistical error.

Also note that the diffusivity of the third geometry (having the small bumps at the top) is very close to that of the ideal Knudsen scattering law. This is significant for the following reason: For all examples of micro-geometries we have studied that do not have an angle, or corner, at its tip point, the roughness parameter is greater than 1 (1 being, by definition, the smoothness constant for the ideal Knudsen scattering). If this indicates some fundamental constraint on smoothness, then by adding the small bump to the micro-geometry at the bottom of figure 11 we have brought diffusivity close to the minimum value. It should be noted, however, that there are geometries with smoothness less than 1, all of which contain tip corners. The smallest value we have obtained so far occurs for a micro-geometry whose tip point has a cusp. We will study the effect of a tip angle or cusp later in the paper.

Further insight into the shadowing effect can be gained by considering the family of geometries depicted in Figure 12. It consists of two sides (in each period), which we refer to as the small and large bump. The ratio of the height of

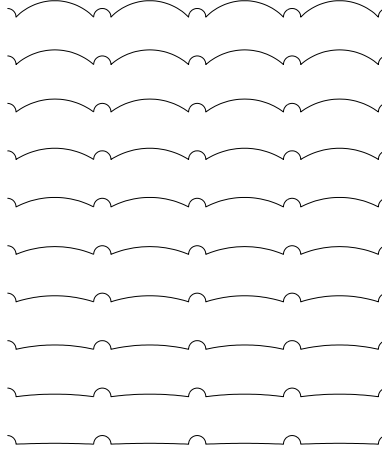


Figure 12: The ratio of the height of the longer bump by the height of the smaller one is  $h$ . The contour at the bottom of the figure corresponds to  $h = 0.1$  and the one at the top to  $h = 1.9$ , increasing in multiples of  $0.2$ .

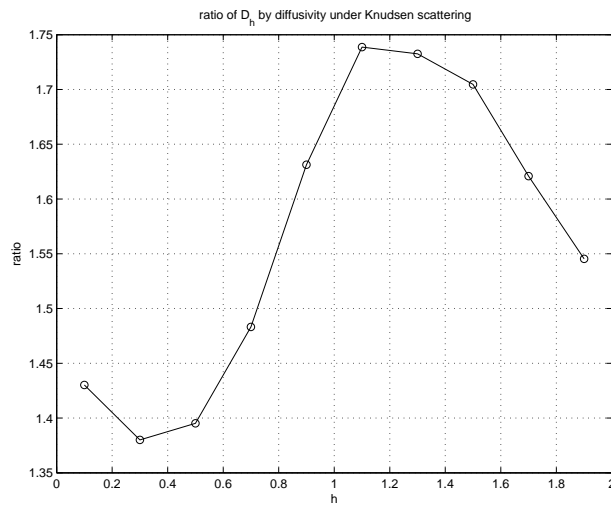


Figure 13: Smoothness  $\mathcal{D}_h/\mathcal{D}_0$  as a function of  $h$ , for the family of micro-geometries of figure 12.

the larger bump by the height of the smaller one is  $h$ . The values of  $\xi_h = \mathcal{D}_h/\mathcal{D}_0$ , where  $\mathcal{D}_h$  is the diffusivity for the geometry having ratio  $h$ , are shown in the graph of Figure 13. This example gives some idea of how different curvatures compete to influence smoothness. The main numerical result is summarized in figure 13.

We observe the following *two-bump effect*: the small bump has a predominant influence on diffusivity for values of  $h$  less than 0.6. (Recall from Section 2.2 that the smaller the radius of curvature the smaller the diffusivity.) As the large bump approaches the small bump in height, its influence on diffusivity quickly becomes more important. This is seen in the fast increase in smoothness for values of  $h$  between 0.6 and 1. For values of  $h$  larger than 1, the parameter  $1+a$  associated to the large bump begins to decrease, causing smoothness to drop.

## 2.4 Effect of a flat exposed side

Before describing the next numerical experiment, we mention a simple scattering model that does not correspond exactly to any micro-geometry but which sheds some light on the phenomenon of this section.

The model is specified by a scattering operator  $P$  given by

$$P_{\text{Maxwell}} = (1 - \alpha)P_\mu + \alpha I,$$

where  $P_\mu$  is the scattering operator for the ideal Knudsen scattering and  $I$  denotes the identity operator, which represents elastic bouncing from a flat wall. Figure 14 is a somewhat fanciful micro-geometry whose scattering operator can be approximated by  $P_{\text{Maxwell}}$ . It consists of a circular cavity carved into a flat mirror-like surface. The inner side of the cavity is lined with some other periodic micro-geometry at a yet smaller scale, which serves to produce fast randomization for a molecule that falls into it. The direction of molecules emerging from the cavity will have, approximately, the ideal Knudsen distribution, the approximation being better the smaller we make the cavity opening. On the other hand, with probability  $\alpha = d/e$ , where  $d$  and  $e = d + o$  are the lengths of flat top and the open side as shown in the figure, an incoming gas molecule will hit the flat side. (See also [Fe].)

Thus the type of scattering represented by  $P_{\text{Maxwell}}$  corresponds to mirror-like reflection with probability  $\alpha$  and, with probability  $1 - \alpha$ , rebounding along a random direction specified by the Knudsen probability law  $\mu$ . This form of scattering was proposed by Maxwell and is well-known in the gas kinetics literature (except for the absence of the exponential term containing the temperature) [C1].

Notice that  $P_\mu$  is the orthogonal projection on the one-dimensional subspace spanned by  $\mu$  in the Hilbert space  $H$  of section 4.3. Then  $P_{\text{Maxwell}} = P_\mu + \alpha P_{\mu^\perp}$ , where  $\mu^\perp$  denotes the subspace of  $H$  orthogonal to  $\mu$ . Therefore, the spectrum of this operator consists of the numbers 1 and  $\alpha$ , the latter with infinite multiplicity. In this case, the so called *spectral gap* is  $1 - \alpha$ . The closer this number is to 1, the faster is the approach to the stationary distribution  $\mu$ .

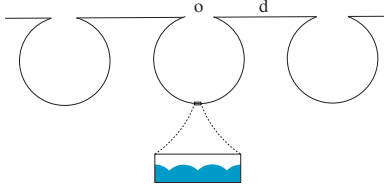


Figure 14: Micro-geometry with scattering operator given approximately by  $P_{\text{Maxwell}}$  with parameter  $\alpha = d/e$ , where  $e = o + d$ .

It can be shown that, for the scattering model  $P_{\text{Maxwell}}$  with eigenvalue  $\alpha$ ,

$$\mathcal{D}_\alpha/\mathcal{D}_0 = \frac{1 + \alpha}{1 - \alpha}. \quad (12)$$

This follows from results in [BGT] and is also discussed in [Fe]. Therefore, this example precisely corresponds to the coin model discussed in the introduction, where  $\alpha$  is the slippage constant.

We now turn to a numerical study of a specific example having both dispersing and mirror-like reflecting sides, and compare it with the ideal case just described. The family of micro-geometries we choose for this purpose is shown in figure 15.

Although the non-flat part of the micro-geometries of figure 15 is very different from that of the ideal scattering cells of figure 14, it may be expected that the latter can serve as a guide for predicting the behavior of the former and other micro-geometries of a similar kind. Based on the above discussion of  $P_{\text{Maxwell}}$ , we expect that  $\mathcal{D}_b/\mathcal{D}_0$  behaves roughly according to the function  $(1 + \alpha)/(1 - \alpha) = 1 + 4b$ , where  $\mathcal{D}_b$  is the diffusivity for the micro-geometry in the flat-top family with parameter  $b$ , where  $b$  is defined in figure 15, and  $\mathcal{D}_0$  is the same for  $b = 0$ . Thus the dependence on  $b$  should be approximately linear, with slope of magnitude roughly comparable to 4. The numerical results are shown in figure 15 and 16.

The smoothness functions are shown in figure 15 and smoothness versus  $b$  is plotted in figure 16. We take the average of  $\xi(x)$  for the last 10 values of  $x$  to represent the smoothness constant. Figure 16 shows the graph of smoothness as a function of the parameter  $b$ . The graph slowly deviates from the linear relation suggested by our analysis of  $P_{\text{Maxwell}}$ , although near  $b = 0$  we have the approximate relation  $\mathcal{D}_b/\mathcal{D}_0 = 1 + 3.4b$ . This is to be compared with the smoothness  $1 + 4b$  described above for the ideal Maxwell model.

## 2.5 Angles and cusps

In this section we try to gain some understanding of how tip angles and cusps affect diffusivity. One reason for giving this geometric feature some attention is that, among all micro-geometries studied in this paper, the smoothness constant attains values smaller than 1 only when the tip (or highest) point has a

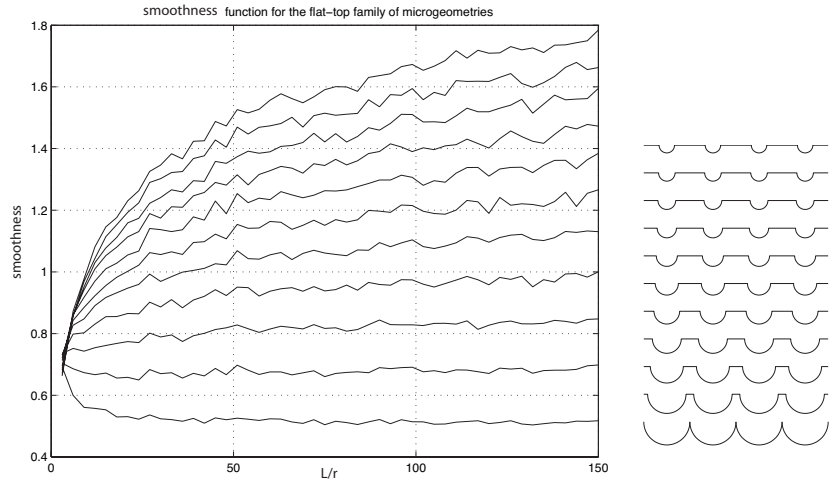


Figure 15: Right-hand side: the *flat-top* family of micro-geometries. The ratio of the length  $d$  of the flat top side by the diameter of the semi-circular cell is  $2b$ , where  $b$  ranges from 0 at the bottom to 1 at the top in steps of 0.1. Left: smoothness function for the flat-top family with parameter  $b$ . Each graph is associated to a micro-geometry in the family on the right in the same order as in the figure. In other words, low values of smoothness correspond to short flat side.

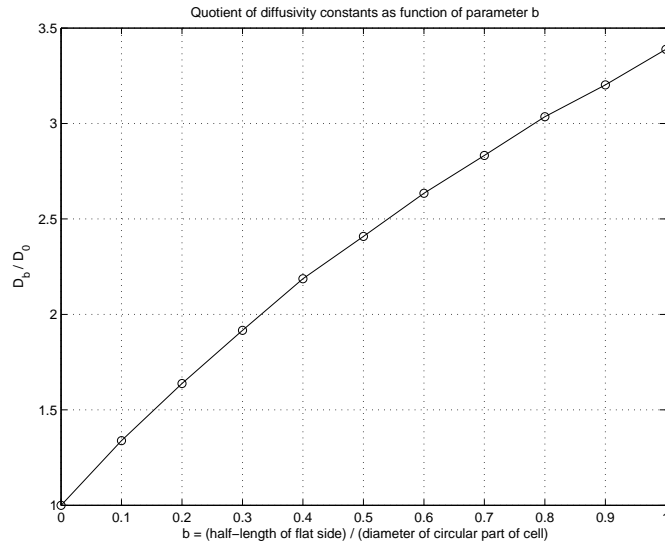


Figure 16: Graph of the quotient of diffusivities  $\mathcal{D}_b/\mathcal{D}_0$  as function of  $b$ .

corner (more precisely, the cell contour is not differentiable there). The smallest value of smoothness we have observed so far occurs when the corner has 0 angle, that is, it is a cusp point. As already pointed out, under the classical Maxwell-Smoluchowski model diffusivity cannot take values less than the Knudsen diffusivity. It is also worth pointing out that, for the two families studied in this section, transition from smoothness less than 1 to greater than 1 occurs when the tip angle is around  $\pi/2$ .

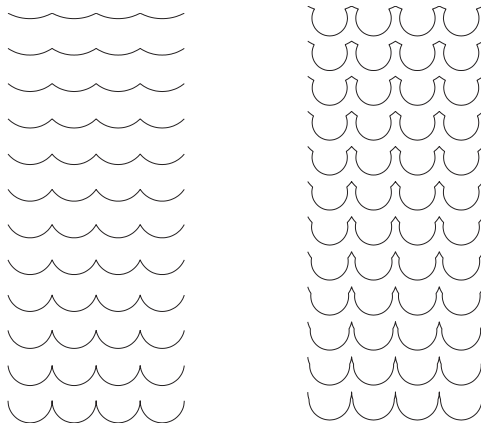


Figure 17: Left: the *wavy* family. The cell boundary is an arc of circle; the tip angle is  $\beta = \pi k/16$ , for  $k = 0, 1, 2, \dots, 11$ . Right: a modified version of the wavy family. The micro-geometries on the right and on the left are the same around the tip point, but those on the right have a circular cavity inserted in the middle of each cell. Common features of smoothness for the two families should reflect the geometric properties around the tip point.

We begin by considering the family of micro-geometries on the left-hand side of figure 17, which we will refer to as the *wavy* family with parameter  $\beta$ . Here, each cell has boundary consisting of a single arc of circle, and the tip point at the juncture of two cells has angle  $\beta = \pi k/16$ , for  $k = 0, 1, \dots, 11$  (from bottom to top). The smoothness function is plotted in figure 18 and the dependence of smoothness on the tip angle is shown in figure 19, with data points marked by circles.

Despite the seeming simplicity of the wavy family, the shape of the graph of figure 19 suggests that other geometric features besides tip angle are competing to control smoothness. For example, for large tip angles, the shadowing effect may not be strong enough to guarantee that regions of the cell away from the tip point are not also affecting smoothness. Furthermore, varying the tip angle also varies the curvature of the cell contour near the tip point. Therefore, it is difficult, without further analysis, to use that graph to infer a general rule for the dependence of smoothness on tip angle. We need to consider other families that can help to extricate these different factors (tip angle, curvature around tip

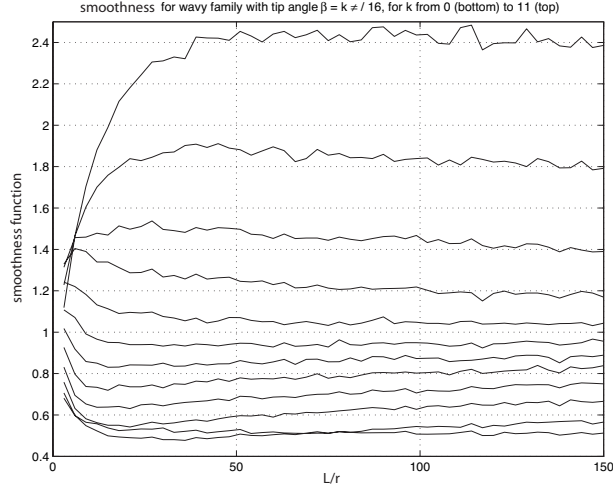


Figure 18: Smoothness function for the wavy family. The order of the graphs correspond to the order of the micro-geometries in figure 17 (left-hand side).

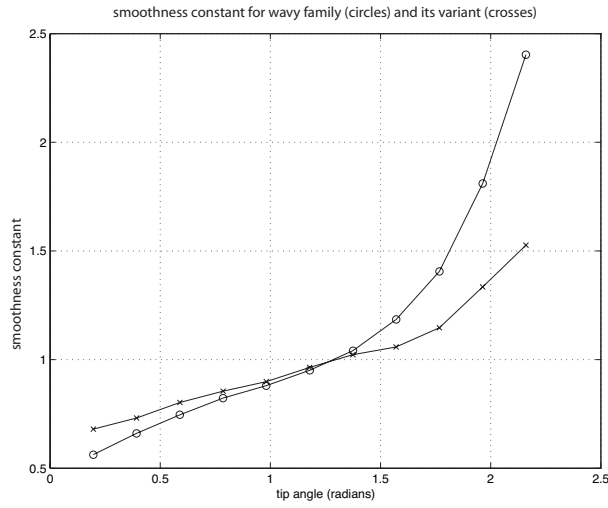


Figure 19: Graph of smoothness constant as function of the tip angle in radians. The tip angle is  $k\pi/16$ , for  $k = 1, 2, \dots, 11$ . Circles are for the family on the left-hand side of figure 17, and crosses are for the family on the right-hand side.

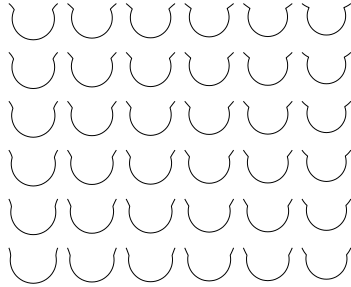


Figure 20: The two-parameter family. Along the horizontal axis (top figure), the radius of curvature takes values:  $-0.5, -1.5, -2.5, 2.5, 1.5, 0.5$  (increasing signed curvature). On the vertical axis, the tip angle takes values  $\beta = k\pi/16$ , for (from bottom to top)  $k = 4, 5, \dots, 9$ . Only one cell of each micro-geometry is shown.

point, not enough shadowing due to excessive “flatness” of the micro-geometry) and to isolate their relative strengths. With this in mind, we first look into the possibility of insufficient shadowing by examining the family on the right-hand side of figure 17. We call this the *modified wavy* family.

Smoothness for the modified wavy family is shown in figure 19 with data points marked by crosses. The graph suggests that for tip angles no greater than about  $\pi/2$ , smoothness is dominated by the geometry around the tip point. For larger angles, the “flatness” of the wavy family begins to assert itself and cause smoothness to grow much faster.

To separate the effects of tip angle and tip curvature, consider the two-parameter family of figure 20. The individual cells on each column have varying tip angle  $k\pi/16$ , where  $k$  varies from 4 at the bottom to 9 at the top. From left to right the radius of curvature are:  $-0.5, -1.5, -2.5, 2.5, 1.5, 0.5$ . (All lengths are given relative to the length of the open side of the cell.)

The graphs of figure 21 give the dependence of smoothness on tip angle for different values of curvature around the tip point. (In order to reduce computer time, we have averaged values over the last 4, rather than the last 10 channel lengths as before. This accounts for the greater fluctuation in the values of smoothness.) One observation that can be made from the graphs of figure 20 is that their linear interpolations have mean slope 0.24 with standard deviation 0.04, while the graph of figure 19 (with points marked with crosses) has slope 0.29 for a linear interpolation over the same range of values of the tip angle. The tentative conclusion is that the change in the radius of curvature near the tip point is of relatively minor importance in accounting for the shape of the graph than the tip angle, at least for not too large tip angles (say, less than  $\pi/2$ ).

Although the dependence of smoothness on tip angle is relatively well approximated by a linear function over the range of angles considered, the dependence on curvature around the tip point is rather more difficult to interpret. We

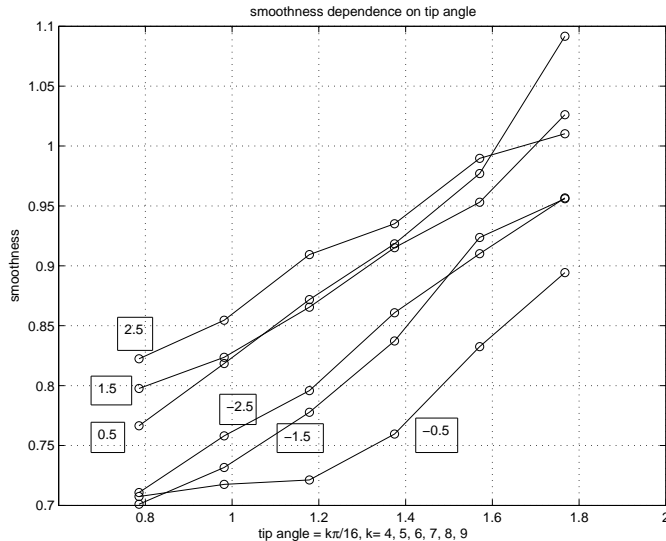


Figure 21: Smoothness as a function of tip angle for each value of the radius of curvature.

need more precise numerical values, or a deeper analytical study, to clarify the meaning and significance of these graphs.

### 3 Collision site statistics

We pointed out in section 1.2.1 the need to estimate the time spent by molecules inside billiard cells. We give below exact values for the mean delay and the mean number of collisions inside a billiard cell in terms of geometric quantities associated to the channel micro-geometry. The results apply to micro-geometries for which the corresponding billiard dynamical system is ergodic. This is the case for most billiard geometries discussed in this paper, which are made of concave, or dispersing, sides. In general, it can be mathematically challenging to determine whether a given geometry corresponds to an ergodic billiard system or not.

It is first necessary to specify the precise way in which those average quantities are defined. Suppose that the billiard cell has total perimeter  $l$ . Let  $e$  be the length of the open side, and  $A$  the enclosed area. Let the open side be parametrized by the interval  $[0, 1]$ . Let  $E = [0, 1] \times [0, \pi]$  be the part of the phase space of the billiard system corresponding to the open side. For each  $(x, \theta) \in E$ , let  $t(x, \theta)$  and  $N(x, \theta)$  be, respectively, the time of first return and the number of collisions before returning to the distinguished side, counting the arrival at the side as one collision. Denote by  $\bar{E}$  the whole unit phase space (i.e., with scalar velocity equal to 1) and define for any  $(p, w) \in \bar{E}$  the function  $s(p, w)$

that gives the time duration of the free flight with (vector) velocity  $w$  from  $p$  to the point of next collision. The average values of  $N$ ,  $t$  are defined by

$$\langle N \rangle_E = \frac{1}{2} \int_0^1 \int_0^\pi N(x, \theta) \sin \theta \, d\theta dx; \quad \langle t \rangle_E = \frac{1}{2} \int_0^1 \int_0^\pi t(x, \theta) \sin \theta \, d\theta dx.$$

Similarly, define the average of  $s$  (over  $\bar{E}$ ), by

$$\langle s \rangle_{\bar{E}} := \int_{\bar{E}} s(\xi) d\bar{\nu}(\xi),$$

where  $\bar{\nu}$  is the normalized Liouville measure on  $\bar{E}$ . With these definitions in place, we can state the main result of this section:

**Theorem 3.1** *Suppose that the billiard system is ergodic. Let  $v$  be the (constant) scalar velocity of the billiard trajectories. Then:*

- $\langle N \rangle_E = l/e;$
- $\langle t \rangle_E = A\pi/ev;$
- $\langle s \rangle_{\bar{E}} = A\pi/lv;$
- $\langle t \rangle_E = \langle N \rangle_E \langle s \rangle_{\bar{E}}$

where  $\langle N \rangle_E$ ,  $\langle t \rangle_E$  and  $\langle s \rangle_{\bar{E}}$  are the mean values of the number or collisions, total time in a cell, and duration of free flight between two collisions with the walls of the cell, respectively.

The proof of theorem 3.1 involves a somewhat standard application of the classical ergodic theorem of Birkhoff, although these relations have not been noted before to the best of our knowledge. The estimation of the number of collisions actually follows from a more elementary recurrence theorem due to M. Kac. (A standard reference is [Pe].) Details are given in [Fe]. We have stated it here for two-dimensional geometries since this is the focus of the present paper, but a similar result holds in dimension 3 by substituting surface area of the cell for the perimeter, volume for area, and area of the open side for the length  $e$ .

Assuming the cosine law, the mean time,  $t_c$ , between consecutive macro-collisions in a 2-dimensional channel of diameter  $d$  is easily calculated to be  $\pi d/(2v)$ . Writing  $t_b = \langle t \rangle_E$ , we obtain  $t_b/t_c = 2A/ed$ . Since  $ed$  is the area of a sector of the channel that lies over a single billiard cell, we have the exact relation:

$$\frac{t_b}{t_c} = 2A_b/A_c, \tag{13}$$

where  $A_c$  is the total area of the channel and  $A_b$  is the part of that area occupied by the billiard cells.

As an illustration of the theorem, we numerically simulate the motion inside the billiard cell for a particular family of micro-geometries and compare the observed mean values with the corresponding values given by the theorem.

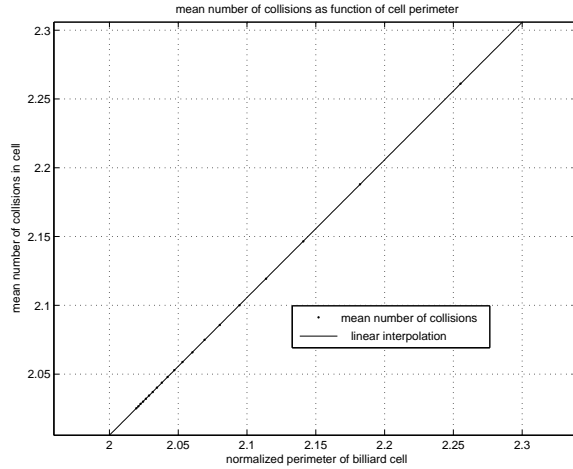


Figure 22: Mean number of collisions in a billiard cell as function of ratio  $l/e$ , for a cell in the bump family and different values of  $a$ . Obtained by simulation of random billiard.

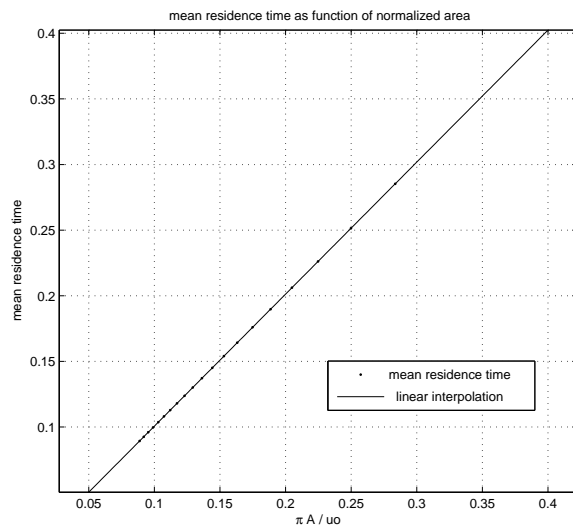


Figure 23: Mean delay time in the billiard cell as a function of  $\pi A/ve$ , again for the bump family. Obtained by simulation of random billiard.

Figure 22 shows the linear dependence of  $\langle N \rangle_E$  on the ratio  $l/e$  and the linear dependence of  $\langle t \rangle_E$  on  $A\pi/2ev$ . The micro-geometry family is that of figure 6, for molecular radius  $A = 0.1, 0.2, \dots, 2.0$  and radius of bump  $R = 1$ . The dots marked on the two graphs are the values obtained by numerically simulating the billiard trajectories. The graphs make it clear that the equalities expressed in the theorem are not approximate relations, but hold exactly.

## 4 Analysis of the scattering operator

The purpose of this section is to describe some general properties of the scattering operator  $P$  introduced in our [FY] and refine some of the results discussed there. In particular, a very general sufficient condition is provided for Knudsen's cosine law to be the limit distribution of post-collision scattered directions. Our discussion will be limited to dimension 2. For more details, the reader should consult [FY].

### 4.1 Random billiards and their scattering operator

It is assumed that the length scale of the micro-geometry is much smaller than the diameter of the channel. Because of this, the reflection law for macro-collisions should be described probabilistically. The channel is then regarded (in this 2 dimensional setting) simply as a pair of straight lines and post-collision directions are specified by a *scattering operator*, which depends on the choice of micro-geometry as explained in [FY]. The scattering operator is obtained as follows: the point along the open side  $e$  (see figure 5) at which the molecule enters the billiard cell is taken to be a random variable distributed uniformly over  $e$ . The direction of reflection after a macro-collision is then given by the angle at which the molecule leaves the cell, which is obtained by following the deterministic, billiard-like flight of the molecule for the given initial direction and random initial position.



Figure 24: The scattering operator for this example is the transition matrix of an ordinary Markov chain with two states,  $\{\theta, \pi - \theta\}$ , where the initial angle satisfies  $0 < \theta < \pi$ . The transition probabilities are given by the diagram on the right. By writing  $2h/(b \tan \theta) = k + s$ , where  $k$  is an integer and  $0 \leq s < 1$ , a simple calculation shows that  $p = s$  if  $k$  is odd and  $p = 1 - s$  if  $k$  is even.

We refer to the scattering operator by  $P$ . In dimension two,  $P$  depends on the angles of incidence,  $\theta_{\text{in}}$ , and reflection,  $\theta_{\text{out}}$ , as already described in section

1. Powers of  $P$  give the distribution of scattered directions after several macro-collisions. For example, for a given initial angle, the probability distribution of angles after three macro-collisions with the channel wall is given by the operator  $P^3$ .

A very simple example illustrating the main points of the model is shown figure 24. Denoting by  $\theta$  the initial angle that a molecular trajectory makes with the axis of the channel, any successive angle must be either  $\theta$  or  $\pi - \theta$ . The transition probabilities are shown in the diagram on the right-hand side of the figure. In this simple case the scattering operator reduces to the transition probability matrix of an ordinary Markov chain.

For most micro-geometries, the scattering operator describes a Markov chain with an infinite set of states parametrized by the reflection angle  $0 < \theta < \pi$ . Figure 25 shows an example with fast randomization, in which a good approximation of Knudsen's law is obtained after only three macro-collisions.

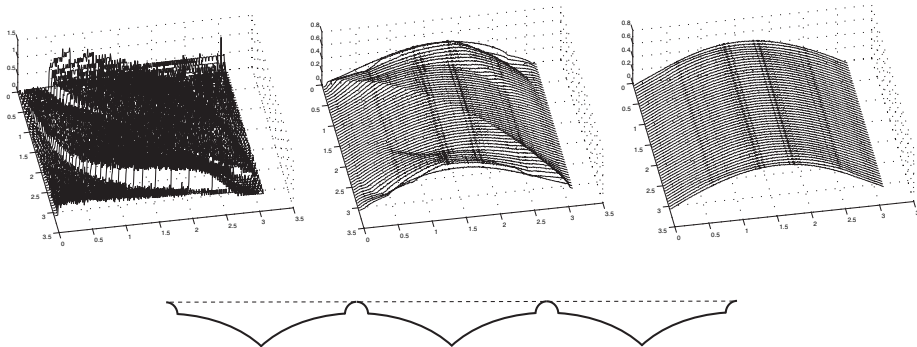


Figure 25: Graphs of the powers  $P, P^2, P^3$ , for the fast randomizing micro-geometry shown at the bottom of the figure. The nearly horizontal axis on the plane of the page measures the angle  $\theta_{\text{out}}$ , and the vertical axis measures  $\theta_{\text{in}}$ . The axis pointing out of the page gives the probability density for the transition  $\theta_{\text{in}} \rightarrow \theta_{\text{out}}$ .

## 4.2 Precise criterion for approach to Knudsen cosine law

The micro-geometry of figure 25 illustrates a central result of [FY]. As the number of collisions increases, the probability density of post-collision distribution of angles after  $n$  collisions approaches the limit  $(1/2) \sin \theta d\theta$ , regardless of the initial distribution of angles. The approach to this universal stationary distribution can be quite fast, as for the micro-geometry of figure 25, or very slow. This is the interpretation of Knudsen's cosine law derived in our [FY] (shown here with a sine function due to the choice of coordinates). As indicated next, this stationary distribution holds fairly generally.

A more formal description of these claims is given next. Let  $\mu$  be the probability measure that assigns probability  $\mu(A) := \frac{1}{2} \int_A \sin \theta d\theta$  to subsets  $A \subset [0, \pi]$ .

- The probability measure  $\mu$  is *stationary* with respect to a random billiard scattering operator  $P$ . In other words, for all events  $A \subset [0, \pi]$  we have  $\mu(A) = \int_0^\pi P(A|\theta) d\mu(\theta)$ , where  $P(A|\theta)$  indicates the conditional probability that the post-collision angle lies in the set  $A$  given that the pre-collision angle is  $\theta$ . (We are using the notation  $d\mu(\theta) = (1/2) \sin \theta d\theta$ .)
- If  $P$  is the scattering operator for an ergodic and aperiodic process (see [Fe] for details), then

$$\lim_{n \rightarrow \infty} P^n(A|\theta) = \mu(A) \tag{14}$$

for all events  $A$  and all  $\theta$  in a set of probability 1.

- A sufficient geometric condition for the above limit to hold (that is, which guarantees that the process is ergodic and aperiodic) is as follows. Suppose that the billiard cell contains a point of maximal height where the surface billiard cell has non-zero curvature. (A point of maximum height is a point on the boundary contour of the billiard cell at which the geometry admits a unique tangent line such that the cell lies entirely on one side of it). Then the associated random billiard admits a unique stationary probability measure, which must be  $\mu$ , and the above limit expression 14 holds.

Figure 26 illustrates the condition for convergence to Knudsen’s cosine law.



Figure 26: The hair-comb microgeometry of figure 24 does not satisfy the ergodicity condition for the validity of Knudsen’s cosine law. For this geometry the probing particle is necessarily point-like (zero radius). But the micro-geometry becomes ergodic if the probing circular molecule has non-zero radius. In this case, the same hair-comb geometry is seen by the molecular center of mass as the thickened contour in the above figure. The tip of the semicircular cap is now a point of maximal height of non-zero curvature. The existence of such a point is sufficient for the cosine law to hold.

### 4.3 The Knudsen spectrum

For random billiards,  $P$  has a number of special properties not shared by general scattering operators. We now describe a few of them. The mathematical details can be found in [FY] and [Fe]. To explain these properties, it is necessary to specify the vector space on which  $P$  acts. We denote by  $H = L^2([0, \pi], \mu)$  the Hilbert space of square integrable functions on the interval  $[0, \pi]$  with respect to the stationary probability measure  $d\mu(\theta) = \frac{1}{2} \sin \theta d\theta$ . The inner product in  $H$  is defined by  $\langle f, g \rangle := \frac{1}{2} \int_0^\pi f(\theta) \bar{g}(\theta) \sin \theta d\theta$ , where  $\bar{g}(\theta)$  denotes complex conjugate of the function  $g$ . It is equivalent, and conceptually helpful, to consider by duality  $P$  as an operator on complex valued measures on  $[0, \pi]$ , whereby  $H$  is

now regarded as the space of densities for such measures. This point of view is more intuitive physically: if a (positive) measure  $\nu$  describes the probability distribution of pre-collision directions, then  $\nu P$  is the probability distribution of directions after collision.

The following properties of  $P$  hold (see [Fe]):

1.  $P$  is a self-adjoint operator on  $H$ . In probabilistic terms, this means that the Markov chain with initial distribution  $\mu$  (the Knudsen distribution) is *reversible*. This is a direct consequence of time reversibility of the corresponding deterministic billiard system. In particular, the spectrum of  $P$  consists of real numbers in the interval  $[-1, 1]$ .
2. If the lines comprising the boundary of a billiard cell are concave, we say that the billiard cell is *dispersing*. For dispersing billiard cells,  $P$  is a *Hilbert-Schmidt* operator. In particular, there exists an orthonormal basis  $\mu_1, \mu_2, \dots$  of  $H$  that diagonalizes  $P$ , so that  $\mu_i P = \lambda_i \mu_i$ , for each  $i$ . It is, therefore, meaningful to speak of the spectrum of eigenvalues of the micro-geometry:  $\lambda_1, \lambda_2, \dots$ . We refer to these numbers as the *Knudsen spectrum* of the micro-geometry.
3. For dispersing micro-geometries, 1 is a non-degenerate eigenvalue of  $P$  associated to the eigenvector  $\mu$ . In other words, the Knudsen distribution is the unique stationary distribution of post-collision directions.

A fundamental quantity derived from the Knudsen spectrum is the *spectral gap*  $\gamma = 1 - \lambda$ , where  $\lambda$  is the largest eigenvalue less than 1. The value of  $\gamma$  controls the rate of convergence of  $P^k$  to  $P_\mu$  as  $k$  increases, where  $P_\mu$  is projection to the orthogonal one-dimensional subspace of  $H$  generated by  $\mu$ .

These results provide a precise understanding of the validity of Knudsen's cosine law: given any initial distribution of directions, say  $\eta$ , the distribution after  $k$  collisions,  $\eta P^k$ , approaches  $\mu$ . This approach is exponentially fast (in the norm of  $H$ ) and the exponent is proportional to the spectral gap  $\gamma$ .

Recall that the operator  $P_{\text{Maxwell}}$  of the idealized example of section 2.4 has spectral gap  $1 - \alpha$ , which is exactly the fraction of diffuse collisions in the Maxwell-Smolukowski model, denoted  $\eta$  at the beginning of section 1. This is an indication that this coefficient can be read from the spectrum of the operator  $P$  of a general micro-geometry.

## 5 Conclusions

This paper set out to determine how the local geometric structure of a macroscopically homogeneous channel influences the diffusivity properties of an inert gas in the Knudsen regime. The interest of such a study is evidenced, for example, by new experimental results showing rapid diffusion in carbon nanotubes [Hol].

We have introduced an idealized experiment in which the flow of gas is recorded at the ends of the channel and the mean residence time of molecules

in the channel is analyzed, for varying channel lengths. We call the experiment and its attendant methodology the *time-of-escape* analysis of gas diffusion. The local geometry of the channel surface, referred to as the channel *micro-geometry*, is encoded in the scattering operator  $P$ . The concept of a random billiard with scattering operator  $P$  was introduced and studied in [FY], and serve as the theoretical basis for the present paper.

The main conclusions pertain to the relationship between geometric features of the surface and a diffusion characteristic of the gas-surface interaction introduced here, which we call the surface *smoothness*,  $\xi$ . This is the ratio of gas diffusivity for the given surface by the diffusivity under ideal Knudsen cosine law of reflection. (It was shown in our previous paper [FY] that the Knudsen cosine law of scattering is the stationary distribution of directions for the scattering operator  $P$  of essentially all micro-geometries; this point is refined in the present paper.) We briefly recall how  $\xi$  is defined in the context of the time-of-escape experiment. The mean time of escape (or residence time),  $\tau$ , regarded as a function of the channel length,  $L$ , the channel radius,  $r$ , and the molecular scalar velocity,  $v$ , has the functional form  $\tau(L, r, v) = \frac{\tau}{v} f(x)$ , where  $x = L/r$  is the dimensionless channel length. We call  $f(x)$  the dimensionless *time-of-escape function*. Information about the transport characteristics of the gas and channel surface are to be extracted from  $f(x)$ . We similarly introduce  $f_0(x)$ , the dimensionless time-of-escape function under the assumption of ideal Knudsen reflection. Finally, we define the smoothness function,  $\xi(x)$ , as the quotient  $\xi(x) = f_0(x)/f(x)$ , and  $\xi$  as the limit of  $\xi(x)$  for large  $x$ . It is explained in the text why  $\xi$  is related to diffusivities as indicated above. Thus a smoothness function greater than (respectively, less than) 1 means that the given micro-geometry promotes (respectively, hinders) diffusional transport compared to the ideal case in which Knudsen cosine law holds exactly at each collision. The quantity  $\xi(x)$  and its limit  $\xi$  reflect purely geometric characteristics of the gas-surface interaction.

We can now enumerate the main geometric features affecting the value of the smoothness constant  $\xi$ .

- The geometric characteristics of the micro-geometry that influence smoothness most strongly are located at the exposed part of the billiard cell. This *shadowing effect*, studied in section 2.3, is quite pronounced. Because of the shadowing effect, we are lead to study the geometric features located on a small neighborhood of the tip point of the micro-geometry: its radius of curvature, length of a flat top, and tip angle.
- The dependence of smoothness on the radius of curvature (appropriately normalized) is fairly regular and well pronounced. For the range of values of channel length studied, the functional relation  $\xi = 1.3(1 + a)$  gives a good approximation. (See section 2.2 for the definition of  $a$  and the precise family of geometries for which this relation is obtained.)
- The effect on smoothness of a flat exposed side is studied in section 2.4, by both numerical and analytical means. It is shown there that smoothness

depends on the (normalized) length of the flat side in a fairly linear way, with a linear coefficient close to 4.

- Our conclusions for the dependence of smoothness on the tip angle are somewhat more tentative, but based on our numerical examples smoothness increases with the tip angle in a fairly regular way, which is close to linear at least for values of the tip angle not exceeding  $\pi/2$ . For sharp angles and cusps it is possible to obtain smoothness values less than one. This is interesting since the value of diffusivity obtained by Smoluchowski based on the classical model of collision introduced by Maxwell predicts that  $\xi$  should not be less than 1.

We also address the question of time delay during macro-collisions. We show that for most micro-geometries (those that define ergodic dynamical systems) the mean delay time,  $\langle t \rangle_E$ , and the mean number of collisions,  $\langle N \rangle_E$ , inside a billiard cell satisfy the exact relations:

- $\langle t \rangle_E = A\pi/ev$ ;
- $\langle N \rangle_E = l/e$ ;

where  $l$  and  $A$  are the perimeter and area of the billiard cell,  $o$  is the length of the open side, and  $v$  is the constant molecular scalar velocity.

We also describe some properties of the scattering operator  $P$  associated to a given micro-geometry. We call the spectrum of eigenvalues of  $P$  the *Knudsen spectrum* of the micro-geometry. A fundamental quantity derived from the Knudsen spectrum is the *spectral gap*,  $\gamma = 1 - \lambda$ , where  $\lambda$  is the largest eigenvalue less than 1. The value of  $\gamma$  controls the rate of convergence of  $P^n \eta$  to the Knudsen distribution  $\mu$ . We expect the smoothness constant for the random flight determined by  $P$  to be very sensitive to  $\gamma$ . More specifically, we expect the smoothness constant  $\xi$  to be roughly proportional to  $1/\gamma$ . This is the case, for example, for the systems studied in section 2.4. There,  $\lambda = \alpha$ , so it follows from the relation  $\xi = (1 + \alpha)/(1 - \alpha)$  in equation 12 that  $\xi = 1/\gamma - 1$ .

There are further observations made during the numerical experiments which we have not discussed here. One observation worth brief mention is that micro-geometries that are not bilaterally symmetric can create a direction bias in the flow of gas, causing more molecules to leave the channel at one of the two ends. This bias can be very pronounced for short channel lengths, but naturally decreases to zero as the length increases.

A question that this paper does not yet address is whether the influence on diffusivity of the geometric factors we have identified can still be detected above the thermal noise due to lattice vibration; in other words, we would like to understand how quickly (in terms of number of collisions) does it take for energy exchange with a channel wall at a given temperature  $T$  to overwhelm any geometric effect we have observed under the conditions of the present study. To address this question, it is necessary to add to our random-billiard scattering operator a noisy term with a temperature dependence and to simulate the time-of-escape experiment for this more refined collision model. It is also of interest to

know how “softening” the hard spheres-type interaction changes our estimates of the smoothness constant  $\xi$ , and how high can it go toward explaining the very large values of  $\xi$  obtained in [Hol]. It is natural to expect that  $\xi$  should increase, but it is not clear, without further work, by how much. It may also be possible to compare some of the theoretical conclusions of the present paper with experimental data from TAP-studies on systems having well defined geometry of loading, such as silicon wafers [W, WCM] for example. We plan to investigate these issues in a future paper.

We wish to thank John T. Gleaves, Guy Marin, Jacob Moulijn, and Freek Kapteijn for fruitful discussions.

## References

- [ACM] G. Arya, H.-C. Chang, and E. J. Maginn. *Knudsen Diffusivity of a Hard Sphere in a Rough Slit Pore*, Physical Review Letters, 91, No. 2, July 2003, 026102(4).
- [Ba] H. Babovsky. *On Knudsen flows within thin tubes*, J. Stat. Phys., 44, Nos. 5/6, 865-878, 1986.
- [BCS] S. K. Bathia, H. Chen, D. S. Sholl. *Comparison of diffuse and viscous contributions to transport coefficients of light gases in single-walled carbon nanotubes*, Molecular Simulation, 31(9):643-649, 2005.
- [BGT] C. Börgers, C. Greengard, and E. Thomann. *The diffusion limit of free molecular flow in thin plane channels*, SIAM J. Appl. Math. 52, No. 4, 1057-1075, 1992.
- [BJN] S. K. Bhatia, O. Jepps, and D. Nicholson. *Tractable molecular theory of transport of Lennard-Jones fluids in nanopores*, Journal of Chemical Physics, V. 120, No. 9, 4472-4485, 2004.
- [C1] C. Cercignani. *The Boltzmann Equation and its Applications*, Springer, New York, 1988. 9
- [C2] C. Cercignani, D. H. Sattinger. *Scaling Limits and Models in Physical Processes*, Birkhäuser, 1998.
- [Co] M.-O. Coppens. 1999, *Catalysis Today* 53, 225-243.
- [Del1] J.A. Delgado, T. A. Nijhuis, F. Kaptein, and I. A. Moulijn. *Determination of adsorption and diffusion parameters in zeolites through structured approach*, Chem. Eng. Sci. 59 (2004) 2477-2487.
- [Del2] J.A. Delgado, T. A. Nijhuis, F. Kaptein, and I. A. Moulijn. *Modeling of fast pulse responses in the Multi-Track: ad Advanced-TAP Reactor*, Chem. Eng. Sci. 57 (2002) 1835-1847.

- [Fe] R. Feres. *Random walks derived from billiards*, preprint, 2004  
<http://www.math.wustl.edu/~feres/publications.html>
- [FY] R. Feres and G. Yablonsky. *Knudsen's cosine law and random billiards*,  
 Chemical Engineering Science 59 (2004) 1541-1556.
- [GYPS] J.T. Gleaves, G. Yablonskii, Y. Schuurman. *TAP-2: An Interrogative  
 Kinetics Approach*, Applied Catalysis: A General 160 (1997) 55-86.
- [Hol] J. K. Holt, H. G. Park, Y. Wang, M. Stadermann, A. B. Artyukhin,  
 C. P. Grigoropoulos, A. Noy, O. Bakajin. *Fast Mass Transport Through  
 Sub-2-Nanometer Carbon Nanotubes*, Science 312 (1034) 2006.
- [JBS] O. G. Jepps, S. K. Bhatia, and D. J. Searles. *Wall mediated transport in  
 confined spaces: Exact theory for low density*, Physical Review Letters,  
 V. 91, No 12, 126102/1-126102/4, 2003.
- [Ke] F. Keil. *Diffusion und Chemische Reaktionen in der Gas/Feststoff*,  
 Katalyse, Springer, 1999.
- [KR] J. Kärgen and D. M. Ruthven. *Diffusion in zeolites and other microporous  
 solids*, Wiley, New York, 1992.
- [Kn] M. Knudsen. *Kinetic Theory of Gases – Some Modern Aspects*,  
 Methuen's Monographs on Physical Subjects, London, 1952.
- [MaCo] K. Malek and M.-O. Coppens. 2001, *Phys. Rev. Lett.* **87**, 125505.
- [Ni] T. A. Nijhuis, L.J.P. van der Broecke, M.J.G. Linders, J.M. van de Graaf,  
 M. Makkee, J.A. Moulijn. *Measurement and Modeling of the transient  
 adsorption, desorption and diffusion processes in microporous material*,  
 Chem. Eng. Sci., 54 (1999) 4423-4436.
- [Pe] K. Petersen. *Ergodic Theory*, Cambridge studies in advanced mathemat-  
 ics 2, Cambridge University Press, 1983.
- [PP] W.G. Pollard and R.D. Present. *On Gaseous Self-Diffusion in Long Cap-  
 illary Tubes*, Physical Review, Volume 73, N. 7, April 1, 1948.
- [SJ] D. S. Sholl, J. K. Johnson. *Making High-Flux Membranes with Carbon  
 Nanotubes*, Science 312 (1003) 2006.
- [Som] G. A. Somorjai, A. M. Contreras, M. Montano, R. M. Rioux. *Clusters,  
 Surfaces and Catalysis*, Proceed. of Nat. Acad. Sci., 103, 28(2006) 10577-  
 10583.
- [SSH] S. B. Santra, B. Sapoval, O. Haeblerlé. *Lévy distribution of collisions for  
 Knudsen diffusion in fractal pores*.
- [WCM] W.L.M. Weerts, M.H.J.M. de Croon, G.B. Marin. *The adsorption of  
 silane, disilane, trisilane on polycrystalline silicon: a transient kinetic  
 study*, Surf. Sci. 367 (1996) 32-339.

- [W] W.L.M. Weerts. *Low Pressure CVD on Polycrystalline Silicon: Reaction Kinetics and Reaction Modelling*, PhD Thesis, University of Eindhoven, 1995.